Small Molecules that Rescue Multiple Phenotypic Aberrations in an iPSC-Derived Neuron Model of CLN3 Disease

One sentence summary: A patient iPSC-derived neuron model of juvenile neuronal ceroid lipofuscinosis was fully characterized and used for drug screening.

Nihar Kinarivala[¶#], Ahmed Morsy[‡#], Ronak Patel[¶#], Angelica V. Carmona[‡], Md. Sanaullah Sajib[¶], Snehal Raut[¶], Constantinos M. Mikelis[¶], Abraham Al-Ahmad[¶*] and Paul C. Trippier[‡,¶,§,*]

[‡]Department of Pharmaceutical Sciences, University of Nebraska Medical Center, Omaha, NE 68198, USA.

[¶]Department of Pharmaceutical Sciences, Texas Tech University Health Sciences Center, School of Pharmacy, Amarillo, TX 79106, USA.

[§]UNMC Center for Drug Discovery, University of Nebraska Medical Center, Omaha, NE 68198, USA.

[#]Contributed equally to this work.

[*]Corresponding Author: paul.trippier@unmc.edu

[*]Corresponding Author: abraham.al-ahmad@ttuhsc.edu

ABSTRACT

The neuronal ceroid lipofuscinoses (NCLs) commonly referred to as Batten disease are a family of rare lysosomal storage disorders (LSDs). The most common form of NCL occurs in children harboring a mutation in the CLN3 gene. This form is lethal with no existing cure or treatment beyond symptomatic relief. The pathophysiology of CLN3 disease is complex and poorly understood, with the current *in vivo* and *in vitro* models failing to identify pharmacological targets for therapeutic intervention. This study reports the characterization of the first CLN3 patient-specific induced pluripotent stem cell (iPSC)-derived model of the blood-brain barrier (BBB) and adds to the few available iPSC-derived neuron models of the disease. Upon differentiation, hallmarks of CLN3 disease were displayed including lipofuscin and subunit C of mitochondrial ATP synthase accumulation, mitochondrial dysfunction and aberrant lysosomal pH. Small molecules were identified that cleared subunit C accumulation by the mTOR-independent modulation of autophagy, conferred protective effects through induction of Bcl-2 and rescued mitochondrial dysfunction.

INTRODUCTION

The neuronal ceroid lipofuscinoses (NCLs) are a family of rare pediatric neurodegenerative diseases that are commonly referred to as Batten disease(*1, 2*). The incidence of the NCLs is estimated at 1 in 12,500 in the United States(*3*). The disease presents with early vision problems and/or seizures which progresses to mental impairment, increased severity seizures, progressive blindness and loss of motor skills. Children at the end-stage of the disease become blind, bedridden, spastic and demented with poorly controlled seizures. Death follows in the teens or early twenties (*2, 4, 5*).

Individual NCLs are classified by the gene that is altered in the disorder, resulting in 13 different subtypes (*2-6*). However, common pathological hallmarks exist across all NCLs. Fat, but primarily protein deposits (termed storage material) build up in the brain, retina, and other tissues. The storage material specifically locates to lysosomes as a secondary effect (*7, 8*). Accelerated apoptosis, impaired autophagy, and secondary destructive inflammation have been documented (*9, 10*). Accumulation of subunit C of mitochondrial ATP synthase in lysosome-derived organelles is a hallmark of the NCLs; however, the exact biochemical mechanism of accumulation is unknown (*8-11*). No cure for the NCLs has yet been realized (*12-16*). However there is one pharmacological intervention available; in 2017 the FDA approved the gene therapy Cerliponase® (Brineura) for CLN2 disease which is an enzyme replacement therapy for tripeptidyl peptidase 1 (TPP1) that can slow or halt progression of the disease (*17*). There is an urgent and unmet medical need for the identification of new drug candidates that are disease-modifying, yet this is hampered by the largely unknown pathophysiology of NCL progression and a lack of phenotypic *in vitro* model systems for drug screening.

The CLN3 subtype of Batten disease, hereto referred to as CLN3 disease, is the most common. Mutations in the CLN3 gene result in reduced production, or dysfunction, of the gene product protein battenin, also referred to as the CLN3 protein, or CLN3P. This protein is primarily located in the membranes surrounding lysosomes. The exact function of battenin is unclear and how this mutation results in expression of the CLN3 phenotype is poorly understood (*18*). The role of apoptosis in neurodegenerative diseases is implicated in neuronal cell death (*19, 20*). Apoptosis, among other cellular death mechanisms, has been proposed as one of the mechanisms of

neuronal death in the NCLs (*21*). One of the known functions of the CLN3 gene, is to modulate the anti-apoptotic protein Bcl-2 (*21-23*). This protein is located to the outer mitochondrial membrane where it plays a key role in regulating cell death by controlling apoptotic protease (caspase) activation (*24*). Small molecules that induce Bcl-2 would partially mimic the function of the native protein. Further, CLN3 is known to modulate endogenous ceramide, resulting in suppression of apoptosis (*23-25*). Defects in autophagy contribute to the neurodegenerative process in many diseases including CLN3 disease (*26*). Accumulation of lipofuscin and subunit C of mitochondrial ATP synthase in the lysosomes of CLN3 disease patients implicates dysfunctional autophagy (*27-29*). Indeed, the lysosomal storage disorders (*30*), such as CLN3 disease, can be thought off as primarily autophagy disorders as lysosomes play a fundamental role in the autophagy pathway by fusing with autophagosomes and digesting their content (*31*). We have previously disclosed compounds designed in our laboratory that are protective in CLN3-patient derived lymphoblasts and healthy IMR90-c4-induced pluripotent stem cell (iPSC)-derived neurons (*32-34*). The compounds upregulate expression of the anti-apoptotic protein Bcl-2 and suppress ceramide levels, directly countering two of the phenotypes of CLN3 disease. These compounds possess a multi-faceted mechanism of action (*35*), also acting to modulate autophagy.

While CLN3-patient-derived lymphoblasts, CLN3 knock-down immortalized cells and primary neurons isolated from CLN3 mouse models provide useful *in vitro* models for pharmacological evaluation, they do not fully recapitulate the phenotype of human CLN3 neurons. The use of iPSCs to model neurodegenerative diseases *in vitro* has gained much recent interest. In particular, several studies highlighted the use of patient-derived iPSCs to model neurodegenerative diseases such as amyotrophic lateral sclerosis, adrenoleukodystrophy, the familial form of Alzheimer's disease, Huntington's disease and Parkinson's disease (*36*). Such models provide a potential alternative to classical approaches. In addition to the presence of a cellular and molecular phenotype in iPSC-derived neurons, several studies have highlighted the presence of an abnormal phenotype at the blood-brain barrier (BBB) upon differentiation of such iPSCs into brain microvascular endothelial cells (BMECs). Thus, the possible identification of a dysfunctional BBB in addition to a more established neuronal phenotype can provide an

inclusive model that can account for assessing the permeability of drug candidates targeting such conditions early in the drug development process (*37*).

Neural progenitor cells (NPCs) differentiated from CLN3 patient-derived iPSCs have been reported to display autophagy dysfunction, lysosomal dysfunction and mitochondrial defects consistent with CLN3 disease. Similarly, CLN2 patient-derived iPSCs possess the TPP1 enzyme deficiency characteristic of CLN2 disease (*38*). In a proceeding study, the CLN3 patient-derived iPSC NPCs were used as a phenotypic model to validate the effect of a small molecule autophagy modifier, identified from a screen conducted in a homozygous Cb*Cln3*$^{\Delta ex7/8}$ cell line stably expressing GFP-LC3 transgene (*29*). Neural stem cells (NSCs) differentiated from CLN1 and CLN2 patient-derived iPSCs were found to exhibit the phenotype of reduced expression of the enzymes palmitoyl-protein thioesterase 1 (PPT1) or TPP1 respectively. These NSCs were used to evaluate the effect of two small molecules versus enzyme replacement therapy (*39*). Neurons differentiated from CLN5 patient-derived iPSCs expressed accumulation of autofluorescent storage material and subunit C of mitochondrial ATP synthase and are being used to further understand the mechanisms of CLN5 disease (*40*). An adeno-associated adenovirus serotype 2 (AAV2) carrying the full-length coding sequence of CLN3 was shown to be effective in restoring full-length CLN3 protein in CLN3 patient iPSC-derived retinal neurons (*41*). Thus, there is a sparsity of characterized CLN3 patient-derived iPSC models that can be differentiated from NSCs to NPCs to mature neurons.

Herein, we report the differentiation and characterization of human CLN3 patient-derived iPSCs through the stages of NSCs, NPCs and ultimately to mature neurons. The reported CLN3 patient iPSC-derived neurons recapitulate several phenotypes of CLN3 disease, including accumulation of autofluorescent lipofuscin and subunit C of mitochondrial ATP synthase, mitochondrial dysfunction and aberrant lysosomal pH. Further, we report the differentiation and characterization of CLN3 patient-derived iPSCs to BMECs. These cells were used to generate a model of the BBB in CLN3 disease for the first time using human iPSC-derived cells. Similar to reports in CLN3 mouse models (*42*), we show an impaired barrier function. We also observed differences in efflux transporter expression between CLN3 and IMR90-c4 control iPSC-derived BMECs and high angiogenic phenotype. Moreover, mature neurons differentiated from CLN3 patient-derived iPSCs were employed to screen

previously identified lead compounds to determine their effect to modulate phenotypic aberrations of CLN3 disease. Three compounds were determined to be novel scaffolds for the design of mammalian target of rapamycin (mTOR)-independent autophagy activators. The compounds significantly induced autophagy in the highly phenotypic CLN3 patient iPSC-derived neuron model system resulting in clearance of subunit C from the neurons. Further, the compounds were shown to induce expression of the protective anti-apoptotic protein Bcl-2 and rescue mitochondrial dysfunction.

RESULTS

iPSC-derived neurons from a CLN3 patient display neuronal phenotype: We first characterized the neuronal differentiation of CLN3 patient iPSCs and compared such differentiation to healthy IMR90-c4 iPSCs (*43*), using a differentiation protocol established by our group and summarized in Figure 1A (*44*), Differentiation of the CLN3-iPSC line into neuronal lineage occurred similarly with the IMR90-c4 iPSC line. The NSCs showed expression of PAX6 (a neuroepithelium marker) by day 10 of differentiation (Fig. 1B), whereas NPCs showed a robust expression of nestin by day 15 of differentiation (Fig. 1C). At day 35 of differentiation (Fig. 1D), both iPSC-derived neuron lines showed the expression of nestin, as well as expression of class III β-tubulin (Tuj1), albeit the immunoreactivity was lower in CLN3-derived neurons compared to IMR90-c4-derived neurons. Expression of MAP2 and NeuN were similar between the two lines, whereas NMDAR2 expression was higher in IMR90-c4-neurons. In conclusion, the presence of the CLN3 mutation appears not to impair the differentiation of iPSCs into neurons as compared to a healthy IMR90-c4 control cell line.

Neurons derived from CLN3 patient iPSCs display increased lipofuscin and subunit C of mitochondrial ATP synthase accumulation in lysosomal and mitochondrial compartments: To assess the presence and localization of lipofuscin in both iPSC-derived neuron lines, detection of autofluorescence was combined with lysosomal staining using Lysotracker®. The CLN3-neurons displayed higher autofluorescence of lipofuscin compared to IMR90-c4-derived neurons (Fig. 2A). Such autofluorescence was particularly co-localized to

lysosomal compartments, suggesting an aggregation and restriction of lipofuscin inclusions in lysosomal compartments. Furthermore, change in lysosomal activity was assessed in both iPSC-derived neuron lines using Lysosensor Green® dye (Fig. 2B). The CLN3-derived neurons displayed a higher acidification of lysosomes compared to control, as reflected by an increased fluorescence intensity. Similar outcomes were observed following treatment with acridine orange (AO, Fig. 2C). Higher acidity of lysosomal pH was observed in CLN3-derived neurons compared to IMR90-c4-derived neurons, as a higher red signal (aggregated AO)/green (oligomeric AO) was observed. Such shift was further aggravated by induction of autophagy via either serum starvation or by treatment with rapamycin at 10 μM. Taken together, this data suggests impaired lysosomal activity in CLN3-derived neurons compared to IMR90-c4-derived neurons.

In addition to changes in lysosomal activity, changes in mitochondrial function were assessed in both IMR90-c4-derived neurons and CLN3-derived neurons (Fig. 3). The CLN3-derived neurons showed higher immunoreactivity to subunit C of mitochondrial ATP synthase and lipofuscin compared to IMR90-c4-derived neurons (Fig. 3A). Although no changes in overall mitochondrial content were observed, a faint immunoreactivity was observed in CLN3-derived neurons (Fig. 3B), suggesting possible impaired mitochondrial function. To assess difference in overall metabolic activity, iPSC-derived neurons were challenged with increasing concentrations of rotenone, a superoxide inducer, (200 and 400 nM concentrations for 24 hours), and changes in cell metabolic activity were measured using MTS reagent (Fig. 3C). Unlike IMR90-c4-derived neurons that showed no differences in cell metabolic activity, CLN3-derived neurons showed a dose-dependent decrease in cell metabolic activity following treatment with rotenone. Such a difference was further demonstrated by changes in mitochondrial superoxide generation using MitoSOX® assay (Fig. 3D, left panel). Under resting conditions, CLN3-derived neurons showed a higher MitoSOX® fluorescence intensity compared to IMR90-c4-derived neurons, suggesting higher production of superoxide free radicals at basal level. Increase in MitoSOX® fluorescence was significant in IMR90-c4-derived neurons following treatment with rotenone at 10 μM and was significant, but remained mild, in CLN3-derived neurons. Similar outcomes were observed by assessing mitochondrial potential using JC-1 staining (Fig. 3D, right panel). The CLN3-derived neurons showed a higher

depolarization status (as reflected by a decrease in red/green JC-1 fluorescence ratio) under resting conditions compared to control. However, no significant differences were observed between these two cell lines following treatment with carbonyl cyanidem-chlorophenylhydrazone (CCCP; an uncoupling agent) at 50 μM. In conclusion, CLN3 mutation appears to impair mitochondrial function and activity in iPSC-derived neurons.

CLN3 mutation is associated with impaired BMEC differentiation: In addition to the effect of CLN3 mutation on iPSC-derived neurons, the presence of a phenotype in non-neuronal cells associated with such mutation was investigated in iPSC-derived BMECs (Fig. 4). Differentiation of iPSCs to BMECs was achieved employing the same differentiation protocol established by Lippmann and colleagues (*45*), commonly used in our studies (*44*) and summarized in Fig. 4A. The BMECs derived from CLN3 patient iPSCs displayed a similar BMEC identity to IMR90-c4-derived BMECs (Fig. 4B), with these cells showing immunoreactivity to vascular markers (PECAM-1, CDH5), as well as the expression of blood-brain barrier selective markers including GLUT1 and the tight junction proteins claudin-5 (CLDN5) and occludin (OCLDN). In addition, both IMR90-c4-derived BMECs and CLN3-derived BMECs showed positive expression (Fig. 4C) for several drug efflux pumps including P-glycoprotein (PGP), breast cancer resistant protein (BCRP) and multidrug resistance protein 1 (MRP). Notably, CLN3-derived BMECs appeared to show higher expression of MRP1 compared to IMR90-c4-derived BMECs, as displayed by a higher immunoreactivity. In conclusion, CLN3-derived BMECs were capable to differentiate and display a BMEC phenotype similar to IMR90-c4-derived BMECs.

CLN3-derived BMECs display an impaired barrier function compared to IMR90-c4-derived BMECs: Differences in barrier function between IMR90-c4-derived BMECs and CLN3-derived BMECs was assessed using transendothelial electrical resistance (TEER) (Fig. 5A) and paracellular permeability using fluorescein (Fig. 5B). The CLN3-derived BMECs displayed a very poor barrier function, with reported TEER in the CLN3-derived BMEC monolayers significantly lower than that of IMR90-c4-derived BMECs (127 ± 31.44 and 1589 ± 470.6 $\Omega.cm^2$ respectively). Such discrepancy between the two monolayers was further confirmed by significant

differences in paracellular permeability between CLN3-derived BMECs and IMR90-c4-derived BMECs (1.364 ± 0.49 x10^{-4} cm/min and 0.64 ± 0.19 x10^{-4} cm/min respectively). Such results suggest that CLN3-derived BMECs have an impaired barrier function. To exclude the possible difference in maturation process between CLN3-derived BMECs and IMR90-c4-derived BMECs as a contributor to this data, an alternative differentiation protocol was set for CLN3-derived BMECs, by extending the UM treatment from 6 days to 7 days and by extending the $EC^{+/+}$ treatment from 2 days to 6 days based on the alternative protocol described by Lippman (*45*). Such extended differentiation protocol also showed impaired barrier function of CLN3-derived BMECs (Fig. 5C), with no significant differences in TEER (62.14 ± 34.16 Ω.cm^2 vs. 48.29 ± 5.21 Ω.cm^2) and fluorescein permeability (5.335 ± 2.639 vs 13.79 ± 7.43 x10^{-4}cm/min) when the two differentiation protocols are compared. The ability of CLN3-derived neurons to induce a barrier phenotype in both IMR90-c4 and CLN3-derived BMECs were assessed by co-culture method. Notably, the presence of CLN3-derived neurons in co-cultures worsened the barrier outcomes in both IMR90-c4-derived BMECs and CLN3-derived BMECs monolayers compared to IMR90-c4-derived neuron co-cultures, as a decrease in TEER and increased fluorescein permeability were apparent (Fig. 5D). In conclusion, our data suggest that the presence of CLN3 mutation may impair BMEC differentiation and barrier induction by neurons.

CLN3 mutation does not affect efflux pump expression and activity: To further demonstrate that such impaired barrier function in BMEC monolayers was associated with impaired drug transport activity, changes in drug efflux pump expression and activity was determined (Fig. 5E&F). The CLN3-derived BMECs displayed higher PGP expression and lower BCRP expression compared to IMR90-c4-derived BMECs. However, no differences in drug efflux pump activity were observed between the two BMEC monolayers. In addition, trafficking of larger molecules such as bovine serum albumin (BSA) and transferrin (Tf) were assessed between the two monolayers (Fig. 5G&H). Notably, uptake of both BSA and Tf were higher in CLN3-derived BMECs compared to IMR90-c4-derived BMECs suggesting dysfunctional membrane trafficking in such cells. Such trafficking was temperature sensitive as a significant decrease in BSA and Tf uptake was noted following

incubation at 4 ºC compared to 37 ºC. Finally, to assess the nature of such impaired membrane trafficking, differences in clathrin and caveolin-1 (cav-1) levels were assessed by immunoblot (Fig.5I). We noted lower levels of clathrin in CLN3-derived BMECs compared to IMR90-c4-derived BMECs, whereas no differences in cav-1 were noted. In conclusion, CLN3-derived BMECs barrier dysfunction was associated with impaired clathrin-mediated membrane trafficking.

CLN3-derived BMECs possess a highly angiogenic phenotype: A previous study reported abnormal angiogenic phenotype in iPSC-derived BMECs obtained from Huntington's disease patients (*46*). Changes in angiogenic phenotype were measured in our developed CLN3-derived BMEC model (Fig. 6). Using a scratch assay (Fig. 6A), no differences in migration were noted between IMR90-c4 and CLN3-derived BMECs monolayers, following 12 hours incubation after scratch (50.02 ± 10.94 vs 52.36 ± 13.94% respectively). However, CLN3-derived BMECs displayed a proliferative status compared to IMR90-c4-derived BMECs (100 ± 2.759 vs 197.7 ± 22.01%) after 12 hours, as measured by MTT assay (Fig. 6B). To further determine if such increased proliferation was associated with an angiogenic phenotype, both types of BMECs were plated on Growth Factor-Reduced (RGF) basement membrane extract and assessed for changes in various angiogenic features at different time intervals following seeding (4, 6, 12, 24, 48 and 72 hours; Fig. 6C-E). We further compared if the presence of bFGF or retinoic acid in EC media can affect the outcome of tube formation by performing the assay with $EC^{+/+}$ and $EC^{-/-}$ medium. We observed formation of tube-like structures with both mediums ($EC^{+/+}$ and $EC^{-/-}$) with no marked effect of bFGF or retinoic acid on tube formation (Supplemental Fig. 1A,B). The CLN3-derived BMECs (red) contrasted IMR90-c4-derived BMECs (blue) by displaying an angiogenic phenotype marked by a higher number of nodes and junctions, as well as a higher total length of tube-like structures (Supplemental Fig. 1A&B). In conclusion, CLN3-derived BMECs display an angiogenic phenotype compared to IMR90-c4-derived BMECs.

Small molecules with neuroprotective activity induce autophagy in neurons differentiated from CLN3 patient-specific iPSCs in a mTOR-independent manner: Previous studies employing novel aromatic carbamate analogues demonstrated induction of autophagy in 'neuron-like' PC12 cells (*33*). A selection of aromatic carbamates, including inactive analogues as control, were screened at a concentration of 3 μM in CLN3-derived neurons to determine the translational activity of these molecules (for structures see Supplemental Fig. 2) in a highly phenotypic model. Several molecules demonstrated significant increase in acridine orange staining compared to vehicle, suggesting translational activity to induce autophagy in CLN3-derived neurons (Fig. 7A). Notably, almost all of the screened aromatic carbamates outperformed rapamycin positive control. Further, changes in autophagy for three selected molecules were determined using the more sensitive CytoID stain. All three molecules showed a general trend of modulating autophagy above vehicle control with compound **9h** providing a significant increase (Fig. 7B). To determine the mechanism of autophagy induction, mammalian target of Rapamycin (mTOR) dependency was determined. It has been suggested that mTOR-independent activation of autophagy would be a more relevant therapeutic option for the treatment of neurodegenerative disorders (*47*). Increased expression of the autophagy marker Beclin 1 was observed upon treatment with rapamycin (a known mTOR inhibitor and autophagy modulator) and compounds **9e**, **9h** and **9g** by Western blot, but not with rasagiline (a Bcl-2 inducer but with no known effect to modulate autophagy) (Fig. 7C), further supporting the autophagy induction activity of these compounds. As expected, rapamycin showed a decrease in ratio of phosphorylated p70 s6 kinase to total p70 s6 kinase. A function performed by mTOR and disrupted upon mTOR inhibition. None of the small molecules showed a decrease in ratio of phosphorylated p70 s6 kinase to total p70 s6 kinase, suggesting that these molecules act by mTOR-independent pathways (Fig. 7C). Elevation of autophagy can be cytotoxic to cells and thus we evaluated the cytotoxic effect of aromatic carbamate analogues on CLN3-derived neurons. All compounds at 3 μM were found to be non-toxic based on propidium iodide staining (Supplemental Fig. 3). Gratifyingly, all selected small molecule mTOR-independent autophagy inducers significantly enhanced the clearance of subunit C of mitochondrial ATP synthase from CLN3-derived neurons by

immunoblot (Fig. 7D). In conclusion, small molecule aromatic carbamates are mTOR-independent autophagy modulators that enhance the clearance of subunit C from CLN3-derived neurons.

Neuroprotective small molecules induce expression of the anti-apoptotic protein Bcl-2: Previously conducted experiments using aromatic carbamates demonstrated neuroprotective activity, in part, by inducing the anti-apoptotic protein Bcl-2 (*33*). To determine if the Bcl-2 induction effect translates from low passage 'neuron-like' PC12 cells (*48*) to neurons differentiated from CLN3 patient-specific iPSCs an ELISA was performed (Supplemental Fig. 4). All three small molecules, **9e**, **9g** and **9h** induce significant increase in Bcl-2 expression in CLN3-derived neurons (Fig. 8A), returning expression to comparable levels as IMR90-c4-derived control neurons. Notably CLN3-derived neurons express significantly lower levels of Bcl-2 than IMR90-derived neurons. In conclusion, all three small molecules significantly induce Bcl-2 expression in CLN3-derived neurons to levels greater than healthy IMR90-c4-derived neuron controls and with greater effect than the known Bcl-2 inducer rasagiline.

Neuroprotective small molecules rescue mitochondrial dysfunction in CLN3-derived NPCs: Mitochondrial dysfunction is a hallmark of the NCLs (*49-51*). We determined the mitochondrial respiration of CLN3-derived NPCs and IMR90-c4-derived NPCs on a Seahorse extracellular flux analyzer (Fig. 8B). Basal respiration in CLN3-derived NPCs was significantly lower than in healthy IMR90-c4-derived control NPCs (Fig. 8C). This level was increased, but not significantly, by treatment of the CLN3-derived NPCs for 48 hours with the maximum non-toxic concentration of rapamycin (0.5 μM) and restored to healthy IMR90-c4-derived NPCs levels by compound **9e** (3 μM), with similar effects observed on spare respiratory capacity (Fig. 8D). Production of ATP in CLN3-derived NPCs trended lower than that of IMR90-c4-derived NPCs. Treatment of CLN3-derived NPCs with Rapamycin (0.5 μM) increased ATP production, but not significantly, with levels being restored to above

IMR90-c4-derived NPCs controls with **9e** (3 μM) after 48 hours incubation (Fig. 8E). In conclusion, compound **9e** rescues the dysfunctional mitochondrial phenotype of CLN3-derived NPCs.

DISCUSSION

The NCLs are a set of neurodegenerative diseases marked by an irreversible and progressive onset ultimately resulting in death. To date, there are no curative treatments available. A major pitfall in developing pharmacological intervention for the NCLs is the limited repertoire of *in vitro* models suitable for the screening of novel neuroprotective drug candidates. The emergence of iPSC-based models has revolutionized the field of disease modeling, resulting in deeper insight into the pathological mechanisms of several neurological diseases including Batten disease (*28, 36, 40*). In this study, we are the first to report the successful differentiation of neurons and BMECs from a patient-derived iPSC line originating from a 21-year-old male bearing a 1kb deletion in the CLN3 gene and heterozygous for E13 c.988G>T, p.Val330Phe mutation, using established protocols (*44, 45*). The BMECs and neurons were fully characterized against the IMR90-c4 iPSC line.

The CLN3 patient iPSC-derived cells recapitulated several phenotypic hallmarks of CLN3 disease; the inclusion of lipofuscin within lysosomes, the accumulation of subunit C of ATP synthase above that of control cells, mitochondrial impairment, and alteration of lysosomal pH. Another key characteristic observed in CLN3 disease is the accelerated apoptosis of neurons (*52*). Cells with CLN3 knocked down, demonstrate diminished expression of Bcl-2, indicating a role for the CLN3 protein in Bcl-2 regulation and apoptosis control (*53*). Reduced expression of Bcl-2 compared with IMR90-c4-derived controls was observed in this iPSC-derived neuron model.

In addition to neuronal features observed in CLN3-derived neurons, we also noted an impaired phenotype in BMECs derived from the CLN3 iPSCs compared to IMR90-c4 iPSCs. We observed a decreased barrier function indicative of increased permeability of the BBB, in particular to the uptake of large molecules at the barrier. Such observation was consistent with the existing literature, as Tecedor and colleagues reported impaired

membrane trafficking in brain endothelial cells transfected with a mutant CLN3 gene (*54*), whereas Saha and colleagues reported an increased permeability in an *in vivo* model of CLN1 disease (*55*). The level of tight junction proteins and abnormalities in claudin-5 levels observed in CLN3-derived BMECs partly explains reduced barrier tightness. Such studies on BBB modeling of rare diseases utilizing iPSCs provides scalable and reproducible human disease models (*46, 56*). This report also highlights that BMECs show expression and activity of efflux transporters including P-gp, BCRP and MRP-1. Prior studies have suggested impaired membrane dynamics and endocytic pathways in Batten disease BMECs, although our model of CLN3 BMECs did not show any such phenotype and presented healthy endocytic transport.

Such observation is important and in agreement with other studies reporting an altered BBB function in other neurological diseases including Adrenoleukodystrophy (ALD) (*57*) and Huntington's disease.(*46*) As reported by Lim and colleagues, we noted an increased angiogenic phenotype in CLN3-derived BMECs compared to control BMECs, suggesting that CLN3 may be associated with signaling pathways involved in angiogenesis and/or barriergenesis. Highly angiogenic vessels impart towards leaky vessels and reduced BBB tightness which is detrimental in multiple disease conditions (*46, 58, 59*). Herein we report the first indication of increased angiogenesis in CLN3-derived BMECs. In agreement with the literature, the co-culture of CLN3-derived neurons with IMR90-c4-derived BMECs was sufficient to worsen barrier function, suggesting the importance of the inclusion of neurovascular coupling when modeling neurological diseases *in vitro*. More investigation into the pathways responsible for increased angiogenesis may help understand and provide methods to counter barrier break down in CLN3 disease.

Presented herein, to the best of our knowledge, is the first report of using mature neurons derived from CLN3 patient iPSCs for a small molecule screen. Lojewski *et al*. have previously demonstrated development of CLN2 and CLN3 iPSCs using patient fibroblasts and differentiated the iPSCs to neurons. Screening of three small molecules was performed in NPCs differentiated from CLN2 iPSCs, but not mature neurons (*38*). We have previously reported small molecule aromatic carbamates that possess multi-functional neuroprotective activity by inducing Bcl-2 levels and increasing autophagy (*33*). The neuroprotective effect of selected analogues was further

demonstrated in lymphoblasts derived from CLN1, CLN2, CLN3, CLN6 and CLN8 patients (*32*). Here, using neurons differentiated from CLN3 patient iPSCs, we demonstrate that selected compounds from our small molecule library translate their mechanistic effect to induce Bcl-2 and enhance autophagy in a highly phenotypic model of Batten disease. The selected small molecule probes significantly induce expression of the anti-apoptotic protein Bcl-2, resulting in levels comparable to those observed in IMR90-c4-derived control neurons. The three small molecule probes outperformed the positive control compound rasagiline, a clinically available compound with neuroprotective activity.

We show the small molecule probes modulate autophagy in an mTOR-independent manner, a characteristic of several known neuroprotective molecules (*60*). Rapamycin, a known mTOR-dependent activator of autophagy, fails to deliver the same magnitude of autophagy activation in the CLN3 patient-specific iPSC-derived neurons as our developed mTOR-independent activators of autophagy. Likewise, a recent report demonstrates that rapamycin is ineffective at activating transcription factor EB (TFEB), a master regulator of lysosomal pathways, in a CLN3 mouse model due to mTOR-dependence, while mTOR-independent activation of TFEB by trehalose, a small molecule with a sugar structure, promoted cellular clearance and increased survival in *Cln3*$^{\Delta ex7/8}$ mice (*61*). Furthermore, all three probe compounds provided statistically significant clearance of subunit C from CLN3-derived neurons. Thus, the discovery and optimization of mTOR-independent activators of autophagy with 'drug-like' profiles of activity, BBB penetration,(*62*) and stability (Supplemental Fig. 5A-7B) may provide for greater therapeutic effect in this rare disease. Autophagy and Bcl-2 are known to possess interdependency in a physiological setting; Bcl-2 and beclin1 demonstrate protein-protein interaction (PPI) and disruption of this PPI activates autophagy (*63*). Data obtained from trials of two other small molecules; cysteamine bitartrate and *N*-acetylcysteine, in CLN1 disease patients did not support the hypothesis that clearance of storage material (or at least granular osmiophilic deposits (GRODs)) correlates to clinical benefit (*64*). Additionally, it has been suggested that in a CLN6 sheep model, storage body accumulation and neurodegeneration may be independent facets of CLN6 mutation (*65*). Accumulation of lipofuscin has been shown to result in autophagy dysfunction and lower turnover of affected mitochondria. This in turn creates a

feedback loop wherein defective mitochondria produce more reactive oxygen species (ROS; which is observed in our developed model system) that increase lipofuscin accumulation, questioning if activation of autophagy would necessarily clear lipofuscin accumulation (*66*). If the hydrolytic function of the lysosome is irreparably damaged by CLN3 mutation or other pathogenesis event, small molecule autophagy inducers would not be able to induce clearance. Such an eventuality occurred in Nieman Pick Type 1 disease, wherein enhanced autophagic flux failed to clear cholesterol levels (*26*). However, the observed clearance of subunit C demonstrated herein would suggest no irreparable damage.

In addition to the significant effect of **9e** on inducing Bcl-2 expression and autophagy, the small molecule successfully rescued mitochondrial dysfunction of the CLN3-derived NPCs. Basal respiration and ATP production have been reported to be significantly reduced in $Cln3^{\Delta ex7/8}$ mouse model astrocytes (*67*). Basal respiration, spare respiratory capacity and ATP function of the CLN3-derived NPCs were all significantly increased to similar or greater levels as seen in healthy IMR90-c4-derived NPC controls. While study of iPSC-derived neurons obtained directly from patients provide for a highly phenotypic model, they also pose some limitations. These include the absence of other cell types in the model system, such as astrocytes, which likely have a role to play in the disease, the effects of in vivo metabolizing enzymes on our small molecules and the lack of a BBB to penetrate, although our studies have provided the first model of the BBB of Batten Disease brains for further study.

In conclusion, we report the first iPSC-derived model of the blood-brain barrier for CLN3 disease, characterizing a dysfunctional barrier that responds to neuronal co-culture. To the best of our knowledge, this is the first report of employing CLN3 patient iPSC-derived neurons for small molecule screening. The screened small molecules rescue CLN3 neurons from three phenotypic consequences of the disease; upregulating Bcl-2, modulating autophagy resulting in enhanced clearance of subunit C and correction of mitochondrial dysfunction. These results identify small molecule **9e** as a valuable probe compound for further study of CLN3 disease and mTOR-independent autophagy modulation and as a compound for further optimization along the drug discovery pipeline. Development of small molecule therapeutics with multiple mechanisms of action is likely to have a

major impact on the treatment of complicated neurological diseases such as Batten disease. Our study establishes that modulation of autophagy and mitochondrial respiration, and induction of Bcl-2 rescues multiple Batten Disease phenotypes. While the identified compounds show great potential, further studies are needed to determine the pharmacokinetic and pharmacodynamic properties of the small molecules in normal and diseased in vivo models and to develop potentially more effective derivatives for testing in human trials.

MATERIALS AND METHODS

Study design

The objective of this study was to examine the effects of protective compounds in a CLN3 disease patient-specific iPSC-derived neuron model. Current disease models for CLN3 are lacking and no reports exist of screening potential drug molecules in a fully differentiated iPSC-derived neuron model. CLN-3 iPSCs were obtained from the New York Stem Cell Foundation iPS core facility (NYSCF, New York City, NY, USA) originating from a 21-year-old male bearing a 1kb deletion in the CLN3 gene and heterozygous for E13 c.988G>T, p.Val330Phe mutation. We fully characterized these iPSCs through NSCs and NPCs to neurons and to BMECs. The iPSC-derived neurons were characterized for CLN3 phenotype and the BMECs for blood-brain barrier transporters and characteristics compared to control healthy iPSC cells. A targeted library of compounds known to be neuroprotective in immortal cell lines was screened for their ability to rescue phenotypic aberrations of CLN3; elevation of Bcl-2 expression, correction of mitochondrial dysfunction and clearance of subunit c of mitochondrial ATP synthase.

Cell lines: iPS(IMR90)-4 iPSC (RRID: RRID:CVCL_C437) line was purchased from WiCell cell repository (WiCell, Madison, WI, USA; ref. *43*). CLN-3 iPSCs were obtained from the New York Stem Cell Foundation iPS core facility (NYSCF, New York City, NY, USA) originating from a 21-year-old male bearing a 1kb deletion in the CLN3 gene and heterozygous for E13 c.988G>T, p.Val330Phe mutation. Somatic cells used for the

derivation of these iPSC lines were obtained with informed consent of subjects and were approved by the respective repositories institutional review boards. Undifferentiated iPSC colonies were maintained on hPSC-grade growth factor-reduced Matrigel (C-Matrigel; Corning, Corning, MA, USA) in the presence of Essential 8 medium (E8; ThermoFisher, Waltham, MA, USA).

BMECs differentiation: iPSCs were differentiated into BMECs following the protocol established by Lippmann and colleagues (*45, 68*). iPSCs were seeded as single cells on T-Matrigel (Trevigen, Gaithersburg, MD, USA) at a cell density of 20000 cells/cm^2 in E8 supplemented with 10 μM Y-27632 (Tocris, Minneapolis, MN, USA). Cells were maintained in E8 for 5 days prior to differentiation. Cells were maintained for 6 days in unconditioned medium (UM: Dulbecco's modified Eagle's medium/F12 with 15 mM HEPES (ThermoFisher), 20% knockout serum replacement (ThermoFisher), 1% non-essential amino acids (ThermoFisher), 0.5% Glutamax® (ThermoFisher), and 0.1 mM b-mercaptoethanol (Sigma-Aldrich, St. Louis, MO, USA). After 6 days, cells were incubated for 2 days in the presence of EC$^{+/+}$ [EC medium (ThermoFisher) supplemented with 1% platelet-poor derived serum (Alfa-Aesar, ThermoFisher, Haverhill, MA, USA), 20 ng/mL human recombinant basic fibroblast growth factor (Tocris, Abingdon, UK), and 10 μM retinoic acid (Sigma-Aldrich)]. After this maturation process, cells were dissociated by Accutase® (Corning) treatment and seeded as single cells on tissue culture plastic surface coated with a solution of collagen from human placenta (Sigma-Aldrich) and bovine plasma fibronectin (Sigma-Aldrich) (80 μg/cm^2 and 20 μg/cm^2, respectively). Twenty-four hours after seeding, cells were incubated in the presence of EC / (EC medium supplemented with 1% platelet-derived serum). Barrier phenotype experiments were performed 48 h after seeding.

iPSC-derived BMEC barrier function: iPSC-derived BMECs were seeded on Transwells® (polyester, 0.4 μm pore size; Corning) and coated as previously described. iPSC-derived BMECs were seeded at a seeding density of 1x10^6 cells/cm^2. Barrier function was assessed 48 h after seeding for iPSC-derived BMECs monolayers; these time points were determined as the most optimal for achieving the highest barrier tightness. Barrier tightness was measured by assessing both the TEER and paracellular diffusion. TEER was measured using an EVOHM STX2

chopstick electrode (World Precision Instruments, Sarasota, FL, USA). For each experiment, three measurements were performed for each insert, and the average resistance obtained was used to determine barrier function. In experiments involving paracellular diffusion, 10 μM sodium fluorescein (Sigma-Aldrich) was added in the donor (apical) chamber and 100 μL aliquots were sampled from the acceptor (basolateral chamber) every 15 min for up to 60 min. Permeability (Pe) for fluorescein was calculated using the clearance slopes obtained by extrapolation using the following formula:

$$1/(Pe*S)=1/(Pt*S)-1/(Pf*S)$$

with Pt and Pf indicative of the clearance slopes of samples and blank (empty coated) filters and S indicative of the insert surface area (cm^2).

Drug uptake assays: Cells were incubated in the presence of 10 μM rhodamine 123 (Sigma-Aldrich), 10 μM CM-DCFDA (ThermoFisher), 20 μM Hoechst (ThermoFisher) for 1 h in an incubator. In some experiments, cells were preincubated in the presence of 5 μM PSC833 (Sigma-Aldrich), 1 μM Ko143 (Sigma-Aldrich), or 10 μM MK571 (Sigma-Aldrich) for 1 h prior to incubation with fluorescent substrates. Following incubation, cells were quickly washed using ice-cold phosphate-buffered saline (PBS) and lysed using radioimmunoprecipitation assay buffer (ThermoFisher). Fluorescence in cell lysates was assessed using a SynergyMX2 ELISA plate reader (Bio-Tek, Winooski, VT, USA). Relative fluorescence units (RFU) were normalized against the total protein content and the protein level was determined by bicinchoninic acid assay (Pierce, Rockford, IL, USA, ThermoFisher). Fluorescence values (expressed as relative fluorescence unit or RFU) obtained from cell lysates in the absence of inhibitor (named as controls) were normalized to the protein content and expressed as RFU/μg protein.

Scratch plate assay (wound healing): Scratch plate assay was performed as previously described (*46*). BMECs were plated on collagen/fibronectin-coated 12-well plates after differentiation. After 24 hours, the cells reached

100% confluence and the initial scratch/wound was made. There were two images/well that were taken using light microscope at time 0 and 12 hours and six wells were used for each experiment/differentiation.

Proliferation assay: Cell proliferation was assessed through the 3-[4, 5-dimethylthiazol-2-yl]-2, 5-dimethyltetrazolium bromide (MTT) assay, as previously described (*69*). Briefly, cells were seeded at a density of 2.5 x 10^4 cells/well in fibronectin-coated 24-well tissue culture plates. After 24 hours, MTT (5 mg/mL in PBS; Fisher) was added at a volume equal to 1/10 of the medium and plates were further incubated at 37 °C for 2 hours. Cells were washed once with PBS and then diluted in 100 μL/well acidified isopropanol (0.33 mL HCL in 100 mL isopropanol). After thorough agitation, the solution was transferred to a 96-well plate and read in a microplate reader at 570 nm.

In vitro **Matrigel tube formation assay:** The Matrigel tube formation assay was performed as previously described (*70*). Wells of a 96-well plate were coated with 40 μL Growth Factor-Reduced (RGF) basement membrane extract (Trevigen) and incubated for 20 minutes at 37 °C to polymerize. Then, 10^4 cells suspended in EC medium supplemented with 1% PDS ($EC^{-/-}$) were added to each well and incubated at 37 °C. Brightfield images were obtained after 4, 6, 12, 24, 48 and 72 hours of incubation period and were analyzed for the number of nodes, number of junctions and total sprout length, using the 'Angiogenesis analyzer' plug-in of ImageJ software.

BSA and Transferrin uptake assay: Differentiated BMECs were plated at confluence on collagen/fibronectin coated 12 well plates. FITC labeled Bovine serum albumin (FITC-BSA-ThermoFisher) and FITC labeled transferrin (FITC-Tf-ThermoFisher) were incubated at 50 ug/mL concentration on cell monolayers for 25 minutes at 37 °C and 4 °C. Cells were lysed using RIPA buffer (ThermoFisher) and FITC fluorescence was measured in

collected buffer. Raw fluorescence intensity (RFU) was normalized against total protein content estimated in the total cell lysates.

Western blot: Cells were washed once with PBS and lysed with RIPA buffer (ThermoFisher). Proteins were quantified via BCA assay (ThermoFisher-# PI-23221) and were then resolved by SDS-PAGE on 4–20% Tris-Glycine gradient gels (BioRad). After transfer to nitrocellulose membranes, blocking was conducted for 1 h in Tris-buffered saline (10 mM Tris-HCl, 100 mM NaCl, pH7.5) containing 0.1% Tween-20 (TBST) and 1% BSA. Samples were probed overnight at 4 °C with anti-Clathrin (CST-#2410), anti-caveolin (ThermoFisher-#MA3-600), anti-β-Actin (CST-#3700) (Santa Cruz Biotechnology; 155,000) anti-Subunit C (Abcam-# ab181243), anti-Bcl-2 (ThermoFisher-# PA5-27094), anti-Beclin 1 (CST-#3738S) or anti-p70 S6 kinase (CST-#2708T) antibodies diluted in TBST with 1% BSA. After being washed five times with TBST, samples were incubated with a peroxidase-conjugated anti-mouse or anti-rabbit secondary antibody (Life Technologies) for 1 h at room temperature. Protein levels were detected via a Super Signal West Pico Chemiluminescent Substrate (ThermoFisher).

Neuronal differentiation: iPSCs were differentiated into neurons using an adherent three-step differentiation method. Undifferentiated iPSCs were allowed to grow on C-Matrigel for 4 days prior to differentiation. Differentiation of these iPSCs into NSCs was induced using neural induction medium (ThermoFisher) for 11 days (*71*). After the induction period, NSCs were enzymatically dissociated by Accutase® (Corning) and seeded as single cells at a cell density of 1 x 10^5 cells/cm^2 in the presence of 10 μM Y-27632 on C-Matrigel-coated plates. Twenty-four hours after seeding, NSCs were further differentiated into NPCs by incubating them in the presence of neural differentiation medium [human pluripotent stem cell serum-free medium (ThermoFisher), supplemented with 2% bovine serum albumin (ThermoFisher), 1% Glutamax I (ThermoFisher), 10 ng/mL human recombinant brain derived neurotrophic growth factor (ThermoFisher), and 10 ng/mL human recombinant glial-derived

neurotrophic factor (ThermoFisher)] for 5 days (*72*). Neurons were seeded on poly-*D*-lysine (2 μg/cm^2; Sigma, St Louis, MO, USA) / laminin (1 μg/cm^2; Sigma)-coated plates and maintained in neuron maturation medium [NMM: Neurobasal-A medium, 2% B27 supplement (ThermoFisher). Medium was replaced every 2 days for 21 days (*44*).

Immunocytochemistry and flow cytometry: Cells were dissociated with Accutase® and centrifuged at 200 g for 5 min (BD Biosciences, San Jose, CA, USA). Cell pellets were fixed with 4% paraformaldehyde (Electron Microscopy Sciences, Hatfield, PA, USA) or 100% cold methanol (MeOH; Sigma Aldrich). Cells were blocked for 1 h at 25 °C in PBSG [PBS supplemented with 10% normal goat serum (Sigma-Aldrich)] with 0.2% Triton-X100. Cells were incubated overnight in primary antibodies at various dilutions (see Table S1), washed with PBS containing 1% bovine serum album (Sigma-Aldrich), and incubated in the presence of Alexa-Fluor conjugated secondary antibodies (1 : 200; ThermoFisher) for 1 h at 25 °C. Cells were counter-stained with DAPI (40 ,6-diamidino-2-phenylindole) (Sigma-Aldrich) and observed on an Leica DMi-8 inverted epifluorescence microscope (Olympus, Tokyo, Japan). Micrograph pictures were acquired using Leica Suite X acquisition program (Intelligent Imaging Innovations, Denver, CO, USA) and processed using ImageJ (NIH, Bethesda, MD, USA). Flow cytometry samples were acquired and analyzed using a FACSVerse system (BD Biosciences. Relative expression was obtained by subtracting the mean fluorescence index from samples versus the mean fluorescence index from the IgG isotype control.

Lysosomal and mitochondrial staining: MitoTracker™ Deep Red FM (ThermoFisher), JC-1 dye (ThermoFisher), MitoSOX®, Red Mitochondrial superoxide indicator (ThermoFisher), Lysosensor Green® DND-189 (ThermoFisher), Acridine Orange (ThermoFisher) or CYTO-ID (Enzo Life Sciences) were used as per manufacturer's protocol. Appropriate controls as detailed by the supplier were used to validate the method. Upon incubation with aforementioned dyes, cells were subjected to flow cytometric or microscopic analysis using a BD

FACSVerse or Leica DMi8 fluorescence microscope. For Rotenone challenge assay, control and CLN3 neurons were incubated with 200 and 400 nM rotenone for 24 hr and MTT assay (Promega) was performed to assess the metabolic rate. Data was presented as % of untreated control.

Co-culture experiments: Twenty-four hours after purification, iPSC-derived BMECs in Transwell inserts were displaced on top of wells containing 40-day old respective iPSC-derived neurons differentiated as described previously. The apical chamber was maintained in $EC^{-/-}$, whereas the bottom chamber was replaced with fresh NMM. Cells were maintained in co-cultures for 2 days. BMEC monocultures treated with similar conditions were used as controls. After 2 days of co-cultures, changes in barrier function were assessed by TEER and permeability. BMECs monocultures maintained in NMM served as control monocultures to normalize such barrier function.

Acridine Orange Flow Cytometry: After 48 hours of treatment with the indicated compound, neurons differentiated from CLN3 patient specific iPSCs were washed with PBS, and then incubated with 1μg/mL of acridine orange for 30 minutes. The cells were washed using PBS, detached using accutase and washed once again with PBS. The cells were resuspended in PBS and 10,000 cells were analyzed using the FITC-A and PerCP-Cy5.5A filter. Data was analyzed using FlowJo v10.2 (FlowJo, LLC) after removing cell debris.

Bcl-2 ELISA: Neurons differentiated from CLN3 patient specific iPSCs were treated with the selected chemical probe for 48h and changes in Bcl-2 protein levels were determined by an ELISA kit (R&D Systems, DYC827-B) using the manufacturer's recommended protocol. Neurons differentiated from IMR90-c4 iPSCs were used as control and followed the same procedure. Briefly, cells were washed once with PBS and then lysed using RIPA buffer (ThermoFisher). The proteins were quantified by BCA assay (ThermoFisher-# PI-23221). Proteins were then normalized to 30 mcg of protein per sample to be used in Bcl-2 protein quantification.

Subunit C expression: Neurons differentiated from IMR90-c4 or CLN3 patient specific iPSCs were treated with the selected chemical probe for 48 hrs. Cells were then washed once with PBS and lysed with RIPA buffer (Thermofisher). Proteins were quantified via BCA assay (Thermofisher-# PI-23221). Normalized protein (30 mcg per sample) was then resolved by SDS-PAGE on 4–20% Tris-Glycine gradient gels (BioRad) and Western blot was performed using Anti-Subunit C (Abcam-# ab181243) antibody diluted in TBST with 1% BSA (1:1000). After being washed five times with TBST, samples were incubated with a peroxidase-conjugated goat anti-rabbit secondary antibody (Life Technologies-# G-21234) for 1 h at room temperature. Protein levels were detected via a SuperSignal West Pico Chemiluminescent Substrate (Thermofisher-# 34580). Protein band expression was then quantified using ImageJ.

Mitochondrial Stress Test: Neural progenitor cells obtained from IMR90-c4 or CLN3 patient-specific iPSCs were separately plated at a density of 250,000 cells/well in 24-well assay plates (Seahorse Bioscience-# 100850-001) using neuronal differentiation medium supplemented with StemPro™ hESC SFM (Life Technologies-# A1000701), BDNF (Peprotech-# 450-02) and GDNF (Peprotech-# 450-10) and allowed to adapt for two days before treatment was added. After 48 h of treatment, the neuronal differentiation medium was replaced by assay medium consisting of XF Base Medium (Seahorse Bioscience-# 103575-100) supplemented with 10 mM glucose, 10 mM pyruvic acid, and 1 mM *L*-glutamine. Subsequently, the analysis of mitochondrial oxygen consumption rate (OCR) was performed in a Seahorse Bioscience XFe 24 flux analyzer according to the manufacturer's instructions. The OCR values were obtained both during baseline (prior to addition of any Mito Stress Test substances), and after the addition of 1.5 μM oligomycin, 2 μM FCCP and 0.5 μM rotenone + 0.5 μM antimycin A respectively. Prior to analysis, data were corrected by withdrawing non-mitochondrial respiration (measured after the injection of rotenone and antimycin A) from all measured OCR values. After the experiment, cells were lysed using RIPA buffer (Thermofisher) and proteins were quantified via BCA assay (Thermofisher-# PI-23221). Results were normalized to protein concentration of each well to its OCR value.

Propidium iodide toxicity: Neurons derived from CLN3 patient iPSCs were incubated with the indicated compound at 3 μM for 48 hours. Cells were dissociated and incubated with 50 μg/mL PI solution (Life Technologies-# P3566) in NMM medium for 15 minutes at 37 °C. PI Stained cells were analyzed by flow cytometry as previously described (*32*).

Statistical Analysis

Comparison of multiple groups was performed using analysis of variance (ANOVA) followed by Tukey's post hoc test; comparisons between two groups were performed using *t* test. *P* values less than 0.05 were considered significant. Statistical calculations were per- formed using Microsoft Excel or GraphPad Prism Software, version 7.0 (http://graphpad.com/scientific-software/prism/). All data shown are representative of experiments from $n \geq 3$ biologically independent samples (see figure legends). All errors bars represent standard deviation (SD).

REFERENCES AND NOTES

1. K. Kollmann, K. Uusi-Rauva, E. Scifo, J. Tyynela, A. Jalanko, T. Braulke, Cell biology and function of neuronal ceroid lipofuscinosis-related proteins. *Biochim. Biophys. Acta.* **1832**, 1866-1881 (2013).
2. J. W. Mink, E. F. Augustine, H. R. Adams, F. J. Marshall, J. M. Kwon, Classification and natural history of the neuronal ceroid lipofuscinoses. *J. Child. Neurol.* **28**, 1101-1105 (2013).
3. P. Santavuori, Neuronal ceroid-lipofuscinoses in childhood. *Brain Dev* **10**, 80-83 (1988).
4. M. Haltia, H. H. Goebel, The neuronal ceroid-lipofuscinoses: a historical introduction. *Biochim. Biophys. Acta.* **1832**, 1795-1800 (2013).
5. A. Schulz, A. Kohlschutter, J. Mink, A. Simonati, R. Williams, NCL diseases - clinical perspectives. *Biochim. Biophys. Acta.* **1832**, 1801-1806 (2013).
6. S. E. Mole, G. Anderson, H. A. Band, S. F. Berkovic, J. D. Cooper, S. M. Kleine Holthaus, T. R. McKay, D. L. Medina, A. A. Rahim, A. Schulz, A. J. Smith, Clinical challenges and future therapeutic approaches for neuronal ceroid lipofuscinosis. *Lancet. Neurol.* **18**, 107-116 (2019).
7. G. W. Anderson, H. H. Goebel, A. Simonati, Human pathology in NCL. *Biochim. Biophys. Acta.* **1832**, 1807-1826 (2013).
8. D. N. Palmer, L. A. Barry, J. Tyynela, J. D. Cooper, NCL disease mechanisms. *Biochim. Biophys. Acta.* **1832**, 1882-1893 (2013).
9. E. M. Lockhart, D. S. Warner, R. D. Pearlstein, D. H. Penning, S. Mehrabani, R.-M. Boustany, Allopregnanolone attenuates N-methyl-d-aspartate-induced excitotoxicity and apoptosis in the human NT2 cell line in culture. *Neurosci. Lett.* **328**, 33-36 (2002).
10. D. A. Persaud-Sawin, R. M. Boustany, Cell death pathways in juvenile Batten disease. *Apoptosis* **10**, 973-985 (2005).
11. R. M. Boustany, Lysosomal storage diseases--the horizon expands. *Nat. Rev. Neurol.* **9**, 583-598 (2013).
12. J. A. Hobert, G. Dawson, Neuronal ceroid lipofuscinoses therapeutic strategies: past, present and future. *Biochim. Biophys. Acta.* **1762**, 945-953 (2006).
13. M. S. Sands, Considerations for the treatment of infantile neuronal ceroid lipofuscinosis (infantile Batten disease). *J. Child. Neurol.* **28**, 1151-1158 (2013).

14. J. A. Hawkins-Salsbury, J. D. Cooper, M. S. Sands, Pathogenesis and therapies for infantile neuronal ceroid lipofuscinosis (infantile CLN1 disease). *Biochim. Biophys. Acta.* **1832**, 1906-1909 (2013).

15. A. M. Wong, A. A. Rahim, S. N. Waddington, J. D. Cooper, Current therapies for the soluble lysosomal forms of neuronal ceroid lipofuscinosis. *Biochem. Soc. Trans.* **38**, 1484-1488 (2010).

16. N. Kinarivala, P. C. Trippier, Progress in the Development of Small Molecule Therapeutics for the Treatment of Neuronal Ceroid Lipofuscinoses (NCLs). *J. Med. Chem.* **59**, 4415-4427 (2016).

17. A. Schulz, T. Ajayi, N. Specchio, E. de Los Reyes, P. Gissen, D. Ballon, J. P. Dyke, H. Cahan, P. Slasor, D. Jacoby, A. Kohlschutter, C. L. N. S. Group, Study of Intraventricular Cerliponase Alfa for CLN2 Disease. *N. Engl. J. Med.* **378**, 1898-1907 (2018).

18. K. E. Wisniewski, N. Zhong, W. Kaczmarski, A. Kaczmarski, S. Sklower-Brooks, W. T. Brown, Studies of atypical JNCL suggest overlapping with other NCL forms. *Pediatr. Neurol.* **18**, 36-40 (1998).

19. M. P. Mattson, Apoptosis in neurodegenerative disorders. *Nat Rev Mol Cell Biol* **1**, 120-129 (2000).

20. G. Smale, N. R. Nichols, D. R. Brady, C. E. Finch, W. E. Horton, Jr., Evidence for apoptotic cell death in Alzheimer's disease. *Exp. Neurol.* **133**, 225-230 (1995).

21. S. C. Lane, R. D. Jolly, D. E. Schmechel, J. ALroy, R. M. Boustany, Apoptosis as the mechanism of neurodegeneration in Batten's disease. *J. Neurochem.* **67**, 677-683 (1996).

22. S. Dhar, R. L. Bitting, S. N. Rylova, P. J. Jansen, E. Lockhart, D. D. Koeberl, A. Amalfitano, R. M. N. Boustany, Flupirtine blocks apoptosis in batten patient lymphoblasts and in human postmitotic CLN3- and CLN2-deficient neurons. *Ann. Neurol.* **51**, 448-466 (2002).

23. K. Puranam, W. H. Qian, K. Nikbakht, M. Venable, L. Obeid, Y. Hannun, R. M. Boustany, Upregulation of Bcl-2 and elevation of ceramide in Batten disease. *Neuropediatrics* **28**, 37-41 (1997).

24. V. S. Marsden, L. O'Connor, L. A. O'Reilly, J. Silke, D. Metcalf, P. G. Ekert, D. C. Huang, F. Cecconi, K. Kuida, K. J. Tomaselli, S. Roy, D. W. Nicholson, D. L. Vaux, P. Bouillet, J. M. Adams, A. Strasser, Apoptosis initiated by Bcl-2-regulated caspase activation independently of the cytochrome c/Apaf-1/caspase-9 apoptosome. *Nature* **419**, 634-637 (2002).

25. K. L. Puranam, W. X. Guo, W. H. Qian, K. Nikbakht, R. M. Boustany, CLN3 defines a novel antiapoptotic pathway operative in neurodegeneration and mediated by ceramide. *Mol. Genet. Metab.* **66**, 294-308 (1999).

26. E. Seranova, K. J. Connolly, M. Zatyka, T. R. Rosenstock, T. Barrett, R. I. Tuxworth, S. Sarkar, Dysregulation of autophagy as a common mechanism in lysosomal storage diseases. *Essays Biochem.* **61**, 733-749 (2017).

27. Y. Cao, J. A. Espinola, E. Fossale, A. C. Massey, A. M. Cuervo, M. E. MacDonald, S. L. Cotman, Autophagy is disrupted in a knock-in mouse model of juvenile neuronal ceroid lipofuscinosis. *J. Biol. Chem.* **281**, 20483-20493 (2006).

28. S. L. Cotman, J. F. Staropoli, The juvenile Batten disease protein, CLN3, and its role in regulating anterograde and retrograde post-Golgi trafficking. *Clin. Lipidol.* **7**, 79-91 (2012).

29. U. Chandrachud, M. W. Walker, A. M. Simas, S. Heetveld, A. Petcherski, M. Klein, H. Oh, P. Wolf, W. N. Zhao, S. Norton, S. J. Haggarty, E. Lloyd-Evans, S. L. Cotman, Unbiased Cell-based Screening in a Neuronal Cell Model of Batten Disease Highlights an Interaction between Ca2+ Homeostasis, Autophagy, and CLN3 Protein Function. *J. Biol. Chem.* **290**, 14361-14380 (2015).

30. C. Ward, N. Martinez-Lopez, E. G. Otten, B. Carroll, D. Maetzel, R. Singh, S. Sarkar, V. I. Korolchuk, Autophagy, lipophagy and lysosomal lipid storage disorders. *Biochim. Biophys. Acta.* **1861**, 269-284 (2016).

31. A. P. Lieberman, R. Puertollano, N. Raben, S. Slaugenhaupt, S. U. Walkley, A. Ballabio, Autophagy in lysosomal storage disorders. *Autophagy* **8**, 719-730 (2012).

32. J. Makoukji, F. Saadeh, K. A. Mansour, S. El-Sitt, J. Al Ali, N. Kinarivala, P. C. Trippier, R. M. Boustany, Flupirtine derivatives as potential treatment for the neuronal ceroid lipofuscinoses. *Ann. Clin. Transl. Neurol.* **5**, 1089-1103 (2018).

33. N. Kinarivala, R. Patel, R. M. Boustany, A. Al-Ahmad, P. C. Trippier, Discovery of Aromatic Carbamates that Confer Neuroprotective Activity by Enhancing Autophagy and Inducing the Anti-Apoptotic Protein B-Cell Lymphoma 2 (Bcl-2). *J. Med. Chem.* **60**, 9739-9756 (2017).

34. N. Kinarivala, J. H. Suh, M. Botros, P. Webb, P. C. Trippier, Pharmacophore elucidation of phosphoiodyn A - Potent and selective peroxisome proliferator-activated receptor beta/delta agonists with neuroprotective activity. *Bioorg. Med. Chem. Lett.* **26**, 1889-1893 (2016).

35. P. C. Trippier, K. Jansen Labby, D. D. Hawker, J. J. Mataka, R. B. Silverman, Target- and mechanism-based therapeutics for neurodegenerative diseases: strength in numbers. *J. Med. Chem.* **56**, 3121-3147 (2013).

36. M. C. Marchetto, K. J. Brennand, L. F. Boyer, F. H. Gage, Induced pluripotent stem cells (iPSCs) and neurological disease modeling: progress and promises. *Hum. Mol. Genet.* **20**, R109-115 (2011).

37. G. D. Vatine, R. Barrile, M. J. Workman, S. Sances, B. K. Barriga, M. Rahnama, S. Barthakur, M. Kasendra, C. Lucchesi, J. Kerns, N. Wen, W. R. Spivia, Z. Chen, J. Van Eyk, C. N. Svendsen, Human iPSC-Derived Blood-Brain Barrier Chips Enable Disease Modeling and Personalized Medicine Applications. *Cell Stem Cell* **24**, 995-1005 e1006 (2019).

38. X. Lojewski, J. F. Staropoli, S. Biswas-Legrand, A. M. Simas, L. Haliw, M. K. Selig, S. H. Coppel, K. A. Goss, A. Petcherski, U. Chandrachud, S. D. Sheridan, D. Lucente, K. B. Sims, J. F. Gusella, D. Sondhi, R. G. Crystal, P. Reinhardt, J. Sterneckert, H. Scholer, S. J. Haggarty, A. Storch, A. Hermann, S. L. Cotman, Human iPSC models of neuronal ceroid lipofuscinosis capture distinct effects of TPP1 and CLN3 mutations on the endocytic pathway. *Hum. Mol. Genet.* **23**, 2005-2022 (2014).

39. N. Sima, R. Li, W. Huang, M. Xu, J. Beers, J. Zou, S. Titus, E. A. Ottinger, J. J. Marugan, X. Xie, W. Zheng, Neural stem cells for disease modeling and evaluation of therapeutics for infantile (CLN1/PPT1) and late infantile (CLN2/TPP1) neuronal ceroid lipofuscinoses. *Orphanet. J. Rare Dis.* **13**, 54 (2018).

40. K. Uusi-Rauva, T. Blom, C. von Schantz-Fant, T. Blom, A. Jalanko, A. Kyttala, Induced Pluripotent Stem Cells Derived from a CLN5 Patient Manifest Phenotypic Characteristics of Neuronal Ceroid Lipofuscinoses. *Int. J. Mol. Sci.* **18**, (2017).

41. L. A. Wiley, E. R. Burnight, A. V. Drack, B. B. Banach, D. Ochoa, C. M. Cranston, R. A. Madumba, J. S. East, R. F. Mullins, E. M. Stone, B. A. Tucker, Using Patient-Specific Induced Pluripotent Stem Cells and Wild-Type Mice to Develop a Gene Augmentation-Based Strategy to Treat CLN3-Associated Retinal Degeneration. *Hum. Gene. Ther.* **27**, 835-846 (2016).

42. M. L. Schultz, L. Tecedor, E. Lysenko, S. Ramachandran, C. S. Stein, B. L. Davidson, Modulating membrane fluidity corrects Batten disease phenotypes in vitro and in vivo. *Neurobiol. Dis.* **115**, 182-193 (2018).

43. J. Yu, M. A. Vodyanik, K. Smuga-Otto, J. Antosiewicz-Bourget, J. L. Frane, S. Tian, J. Nie, G. A. Jonsdottir, V. Ruotti, R. Stewart, Slukvin, II, J. A. Thomson, Induced pluripotent stem cell lines derived from human somatic cells. *Science* **318**, 1917-1920 (2007).

44. R. Patel, S. Page, A. J. Al-Ahmad, Isogenic blood-brain barrier models based on patient-derived stem cells display inter-individual differences in cell maturation and functionality. *J. Neurochem.* **142**, 74-88 (2017).

45. E. S. Lippmann, S. M. Azarin, J. E. Kay, R. A. Nessler, H. K. Wilson, A. Al-Ahmad, S. P. Palecek, E. V. Shusta, Derivation of blood-brain barrier endothelial cells from human pluripotent stem cells. *Nat. Biotechnol.* **30**, 783-791 (2012).

46. R. G. Lim, C. Quan, A. M. Reyes-Ortiz, S. E. Lutz, A. J. Kedaigle, T. A. Gipson, J. Wu, G. D. Vatine, J. Stocksdale, M. S. Casale, C. N. Svendsen, E. Fraenkel, D. E. Housman, D. Agalliu, L. M. Thompson, Huntington's Disease iPSC-Derived Brain Microvascular Endothelial Cells Reveal WNT-Mediated Angiogenic and Blood-Brain Barrier Deficits. *Cell Rep.* **19**, 1365-1377 (2017).

47. W. E. Hochfeld, S. Lee, D. C. Rubinsztein, Therapeutic induction of autophagy to modulate neurodegenerative disease progression. *Acta. Pharmacol. Sin.* **34**, 600-604 (2013).

48. N. Kinarivala, K. Shah, T. J. Abbruscato, P. C. Trippier, Passage Variation of PC12 Cells Results in Inconsistent Susceptibility to Externally Induced Apoptosis. *ACS Chem. Neurosci.* **8**, 82-88 (2017).

49. R. D. Jolly, S. Brown, A. M. Das, S. U. Walkley, Mitochondrial dysfunction in the neuronal ceroid-lipofuscinoses (Batten disease). *Neurochem. Int.* **40**, 565-571 (2002).

50. K. Luiro, O. Kopra, T. Blom, M. Gentile, H. M. Mitchison, I. Hovatta, K. Tornquist, A. Jalanko, Batten disease (JNCL) is linked to disturbances in mitochondrial, cytoskeletal, and synaptic compartments. *J. Neurosci. Res.* **84**, 1124-1138 (2006).

51. K. Wager, A. A. Zdebik, S. Fu, J. D. Cooper, R. J. Harvey, C. Russell, Neurodegeneration and Epilepsy in a Zebrafish Model of CLN3 Disease (Batten Disease). *PLoS One* **11**, e0157365 (2016).

52. S. C. Lane, R. D. Jolly, D. E. Schmechel, J. Alroy, R. M. Boustany, Apoptosis as the mechanism of neurodegeneration in Batten's disease. *J. Neurochem.* **67**, 677-683 (1996).

53. D. Mao, J. Che, S. Han, H. Zhao, Y. Zhu, H. Zhu, RNAi-mediated knockdown of the CLN3 gene inhibits proliferation and promotes apoptosis in drug-resistant ovarian cancer cells. *Mol. Med. Rep.* **12**, 6635-6641 (2015).

54. L. Tecedor, C. S. Stein, M. L. Schultz, H. Farwanah, K. Sandhoff, B. L. Davidson, CLN3 loss disturbs membrane microdomain properties and protein transport in brain endothelial cells. *J. Neurosci.* **33**, 18065-18079 (2013).

55. A. Saha, C. Sarkar, S. P. Singh, Z. Zhang, J. Munasinghe, S. Peng, G. Chandra, E. Kong, A. B. Mukherjee, The blood-brain barrier is disrupted in a mouse model of infantile neuronal ceroid lipofuscinosis: amelioration by resveratrol. *Hum. Mol. Genet.* **21**, 2233-2244 (2012).

56. G. D. Vatine, A. Al-Ahmad, B. K. Barriga, S. Svendsen, A. Salim, L. Garcia, V. J. Garcia, R. Ho, N. Yucer, T. Qian, R. G. Lim, J. Wu, L. M. Thompson, W. R. Spivia, Z. Chen, J. Van Eyk, S. P. Palecek, S. Refetoff, E. V. Shusta, C. N. Svendsen, Modeling Psychomotor Retardation using iPSCs from MCT8-Deficient Patients Indicates a Prominent Role for the Blood-Brain Barrier. *Cell Stem Cell* **20**, 831-843 e835 (2017).

57. C. A. A. Lee, H. S. Seo, A. G. Armien, F. S. Bates, J. Tolar, S. M. Azarin, Modeling and rescue of defective blood-brain barrier function of induced brain microvascular endothelial cells from childhood cerebral adrenoleukodystrophy patients. *Fluids Barriers CNS* **15**, 9 (2018).

58. Z. G. Zhang, L. Zhang, Q. Jiang, R. Zhang, K. Davies, C. Powers, N. Bruggen, M. Chopp, VEGF enhances angiogenesis and promotes blood-brain barrier leakage in the ischemic brain. *J. Clin. Invest.* **106**, 829-838 (2000).

59. V. Rigau, M. Morin, M. C. Rousset, F. de Bock, A. Lebrun, P. Coubes, M. C. Picot, M. Baldy-Moulinier, J. Bockaert, A. Crespel, M. Lerner-Natoli, Angiogenesis is associated with blood-brain barrier permeability in temporal lobe epilepsy. *Brain* **130**, 1942-1956 (2007).

60. S. Y. Kuo, A. B. Castoreno, L. N. Aldrich, K. G. Lassen, G. Goel, V. Dancik, P. Kuballa, I. Latorre, K. L. Conway, S. Sarkar, D. Maetzel, R. Jaenisch, P. A. Clemons, S. L. Schreiber, A. F. Shamji, R. J. Xavier, Small-molecule enhancers of autophagy modulate cellular disease phenotypes suggested by human genetics. *Proc. Natl. Acad. Sci. U. S. A.* **112**, E4281-4287 (2015).

61. M. Palmieri, R. Pal, H. R. Nelvagal, P. Lotfi, G. R. Stinnett, M. L. Seymour, A. Chaudhury, L. Bajaj, V. V. Bondar, L. Bremner, U. Saleem, D. Y. Tse, D. Sanagasetti, S. M. Wu, J. R. Neilson, F. A. Pereira, R. G. Pautler, G. G. Rodney, J. D. Cooper, M. Sardiello, mTORC1-independent TFEB activation via Akt inhibition promotes cellular clearance in neurodegenerative storage diseases. *Nat. Commun.* **8**, 14338 (2017).

62. P. C. Trippier, Selecting Good 'Drug-Like' Properties to Optimize Small Molecule Blood-Brain Barrier Penetration. *Curr. Med. Chem.* **23**, 1392-1407 (2016).

63. M. C. Maiuri, E. Zalckvar, A. Kimchi, G. Kroemer, Self-eating and self-killing: crosstalk between autophagy and apoptosis. *Nat. Rev. Mol. Cell. Biol.* **8**, 741-752 (2007).

64. S. W. Levin, E. H. Baker, W. M. Zein, Z. Zhang, Z. M. Quezado, N. Miao, A. Gropman, K. J. Griffin, S. Bianconi, G. Chandra, O. I. Khan, R. C. Caruso, A. Liu, A. B. Mukherjee, Oral cysteamine bitartrate and N-acetylcysteine for patients with infantile neuronal ceroid lipofuscinosis: a pilot study. *Lancet Neurol.* **13**, 777-787 (2014).

65. M. J. Oswald, D. N. Palmer, G. W. Kay, S. J. Shemilt, P. Rezaie, J. D. Cooper, Glial activation spreads from specific cerebral foci and precedes neurodegeneration in presymptomatic ovine neuronal ceroid lipofuscinosis (CLN6). *Neurobiol. Dis.* **20**, 49-63 (2005).

66. A. Terman, T. Kurz, M. Navratil, E. A. Arriaga, U. T. Brunk, Mitochondrial turnover and aging of long-lived postmitotic cells: the mitochondrial-lysosomal axis theory of aging. *Antioxid. Redox. Signal* **12**, 503-535 (2010).

67. M. E. Bosch, T. Kielian, Astrocytes in juvenile neuronal ceroid lipofuscinosis (CLN3) display metabolic and calcium signaling abnormalities. *J. Neurochem.* **148**, 612-624 (2019).

68. E. S. Lippmann, A. Al-Ahmad, S. M. Azarin, S. P. Palecek, E. V. Shusta, A retinoic acid-enhanced, multicellular human blood-brain barrier model derived from stem cell sources. *Sci. Rep.* **4**, 4160 (2014).

69. G. Kokolakis, C. Mikelis, E. Papadimitriou, J. Courty, E. Karetsou, P. Katsoris, Effect of heparin affin regulatory peptide on the expression of vascular endothelial growth factor receptors in endothelial cells. *In Vivo* **20**, 629-635 (2006).

70. C. Mikelis, M. Lamprou, M. Koutsioumpa, A. G. Koutsioubas, Z. Spyranti, A. A. Zompra, N. Spiliopoulos, A. A. Vradis, P. Katsoris, G. A. Spyroulias, P. Cordopatis, J. Courty, E. Papadimitriou, A peptide corresponding to the C-terminal region of pleiotrophin inhibits angiogenesis in vivo and in vitro. *J. Cell Biochem.* **112**, 1532-1543 (2011).

71. Y. Yan, S. Shin, B. S. Jha, Q. Liu, J. Sheng, F. Li, M. Zhan, J. Davis, K. Bharti, X. Zeng, M. Rao, N. Malik, M. C. Vemuri, Efficient and rapid derivation of primitive neural stem cells and generation of brain subtype neurons from human pluripotent stem cells. *Stem Cells Transl. Med.* **2**, 862-870 (2013).

72. A. Efthymiou, A. Shaltouki, J. P. Steiner, B. Jha, S. M. Heman-Ackah, A. Swistowski, X. Zeng, M. S. Rao, N. Malik, Functional screening assays with neurons generated from pluripotent stem cell-derived neural stem cells. *J. Biomol. Screen.* **19**, 32-43 (2014).

ACKNOWLEDGEMENTS

Funding: This work was funded by the National Center for Advancing Translational Sciences of the National Institutes of Health under Award UL1TR001105 (P.C.T.). The content is solely the responsibility of the authors and does not necessarily represent the official views of the NIH. The authors are grateful to Texas Tech University Health Sciences Center (M.S., A.A-A. and P.C.T) and the University of Nebraska Medical Center (P.C.T) for funding support. **Author contributions:** N.K. grew and differentiated cells, synthesized compounds, performed autophagy experiments and Bcl-2 experiments and analyzed results. A.M. grew and differentiated cells, synthesized compounds, performed subunit c clearance experiments, Bcl-2 experiments and the mitochondrial stress test and analyzed results. R.P. grew, differentiated and characterized cells, performed BBB characterization and transporter experiments and analyzed results. A.V.C. synthesized compounds and performed NMR stability studies. M.S.S. performed angiogenic characterization. S.R. grew and differentiated cells. C.M. oversaw experimental design of the angiogenic characterization and analyzed data. A. A-A. oversaw experimental design of stem cell studies, initiated and supervised the BBB experiments, interpreted data and wrote the manuscript with input from all coauthors. P.C.T. conceived, initiated, supervised the project, analyzed data and wrote the manuscript with input from all coauthors. **Competing interests:** N.K. and P.C.T are inventors on a patent application (PCT Int. App. WO 2019014547) submitted by Texas Tech University that covers the composition of matter of the compounds described herein. P.C.T. serves as an advisor to Circumvent Pharmaceuticals Inc. **Data and materials available:** All data associated with this study are present in the paper or the supplemental material. Requests for compound samples may be made to P.C.T.

Figure 1: Cellular phenotyping of iPSC-derived neurons.

(A) Diagram of the differentiation protocol used in this study. (B) Expression of the neuroepithelial marker PAX6 of iPSC-derived neural stem cells (NSCs) from IMR90-c4 and CLN3 iPSC lines. (C) Expression profile of nestin and doublecortin (DCX) in neural progenitor cells (NPCs) derived from IMR90-c4 and CLN3 iPSC lines. (D) Neuronal phenotype of iPSC-derived neurons at 30 days of differentiation. Differential expression of class III β-tubulin (Tuj1) in IMR90-c4-neurons compared to CLN3-neurons.

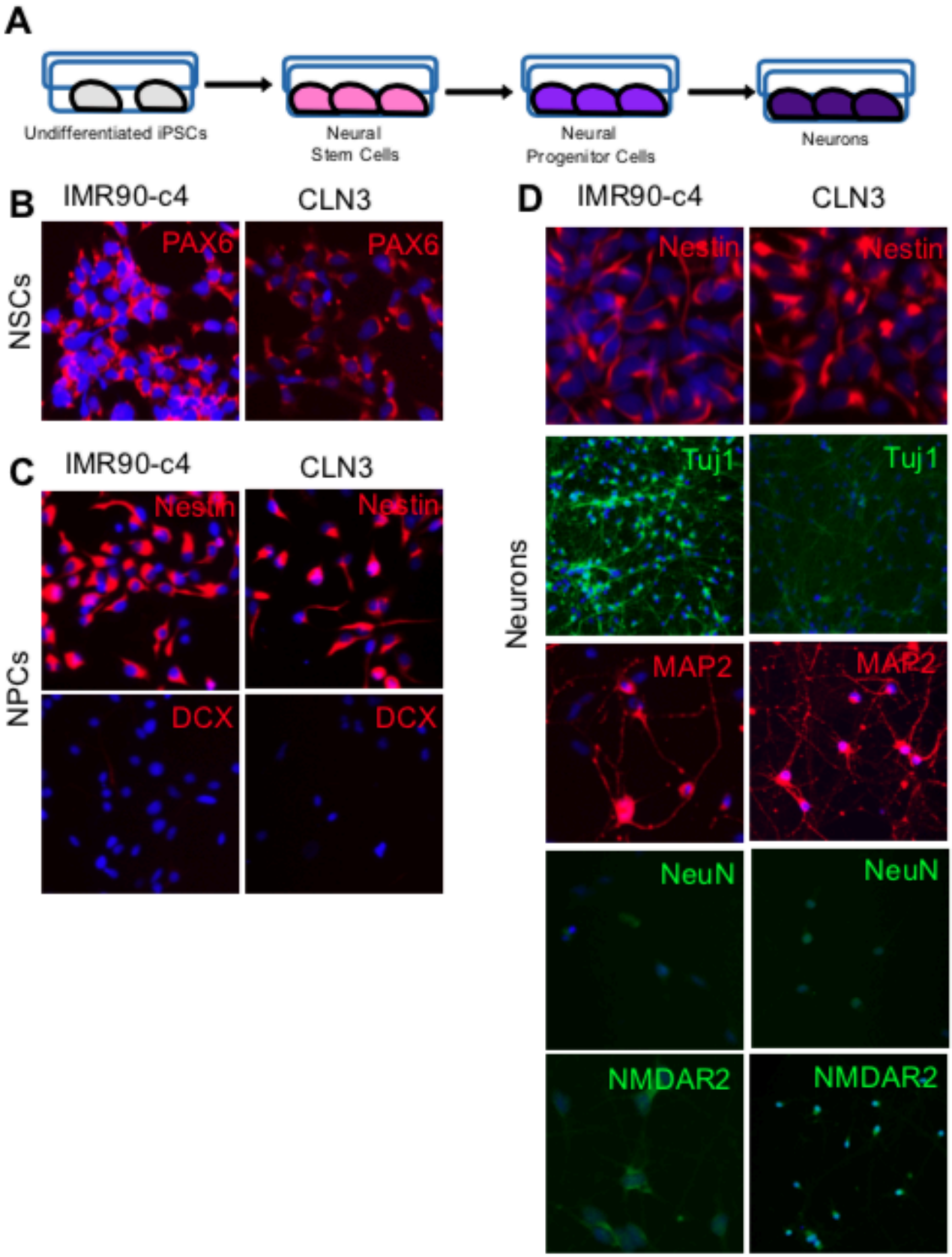
A
Undifferentiated iPSCs
Neural Stem Cells
Neural Progenitor Cells
Neurons
B
IMR90-c4
CLN3
NSCs
PAX6
PAX6
C
IMR90-c4
CLN3
NPCs
Nestin
Nestin
DCX
DCX
D
IMR90-c4
CLN3
Nestin
Nestin
Neurons
Tuj1
Tuj1
MAP2
MAP2
NeuN
NeuN
NMDAR2
NMDAR2

Figure 2: CLN3-neurons display lipofuscin inclusion and impaired lysosomal activity

(A) Representative micrograph picture of iPSC-derived neurons stained with Lysotracker® and lipofuscin autofluorescence. (B) CLN3-derived neurons (red bar) have a higher number of acidic lysosomes compared to IMR90-c4-derived neurons (blue bar). Representative micrograph picture of Lysosensor® Green. Semi-quantitative analysis of Lysosensor® Green fluorescence following incubation of live cells with 100 nM Lysosensor® dye. (C) Acridine orange (AO) fluorometric ratio in IMR90-c4 and CLN3-derived neurons following autophagy induction by 10 μM rapamycin or serum-starvation treatment. N=3/group, * denotes P<0.05, ** denotes P<0.01.

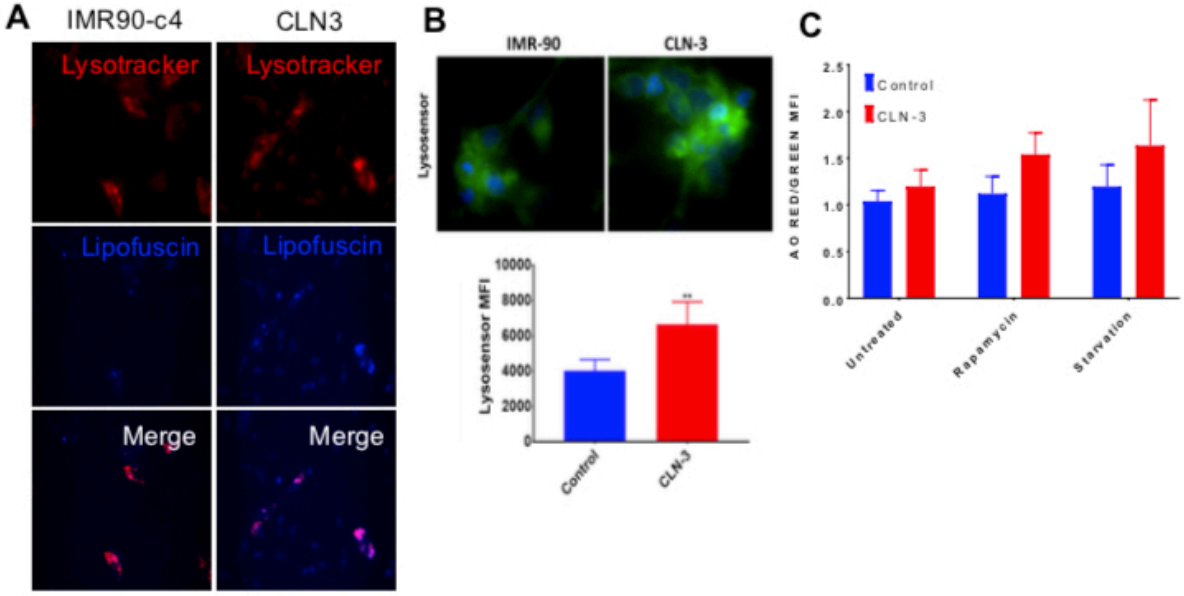
A
IMR90-c4
CLN3
Lysotracker
Lysotracker
Lipofuscin
Lipofuscin
Merge
Merge
B
IMR-90
CLN-3
Lysosensor
Lysosensor MFI
10000
8000
6000
4000
2000
0
**
Control
CLN-3
C
AO RED/GREEN MFI
2.5
2.0
1.5
1.0
0.5
0.0
Control
CLN-3
Untreated
Rapamycin
Starvation

Figure 3: CLN3-derived neurons show impaired mitochondrial function.

(A) Representative micrograph pictures of IMR90-c4 and CLN3-derived neurons staining for subunit C. (B) MitoTrackerTM® (green) micrograph picture (blue=DAPI). (C) Cell metabolic activity following rotenone treatment using an MTS-based assay. Absorbance was normalized to untreated cells. (D) Mitochondrial oxidative stress and activity measured by MitoSOX® and JC-1 dye fluorescence under control condition and following treatment with 10 μM rotenone for 10 minutes (left) or incubation with 50 μM treatment of carbonyl cyanidem-chlorophenylhydrazone (CCCP) (right). N=3/group, * and # denotes P<0.05, ** P<0.01, ***P<0.001 and ****P<0.0001.

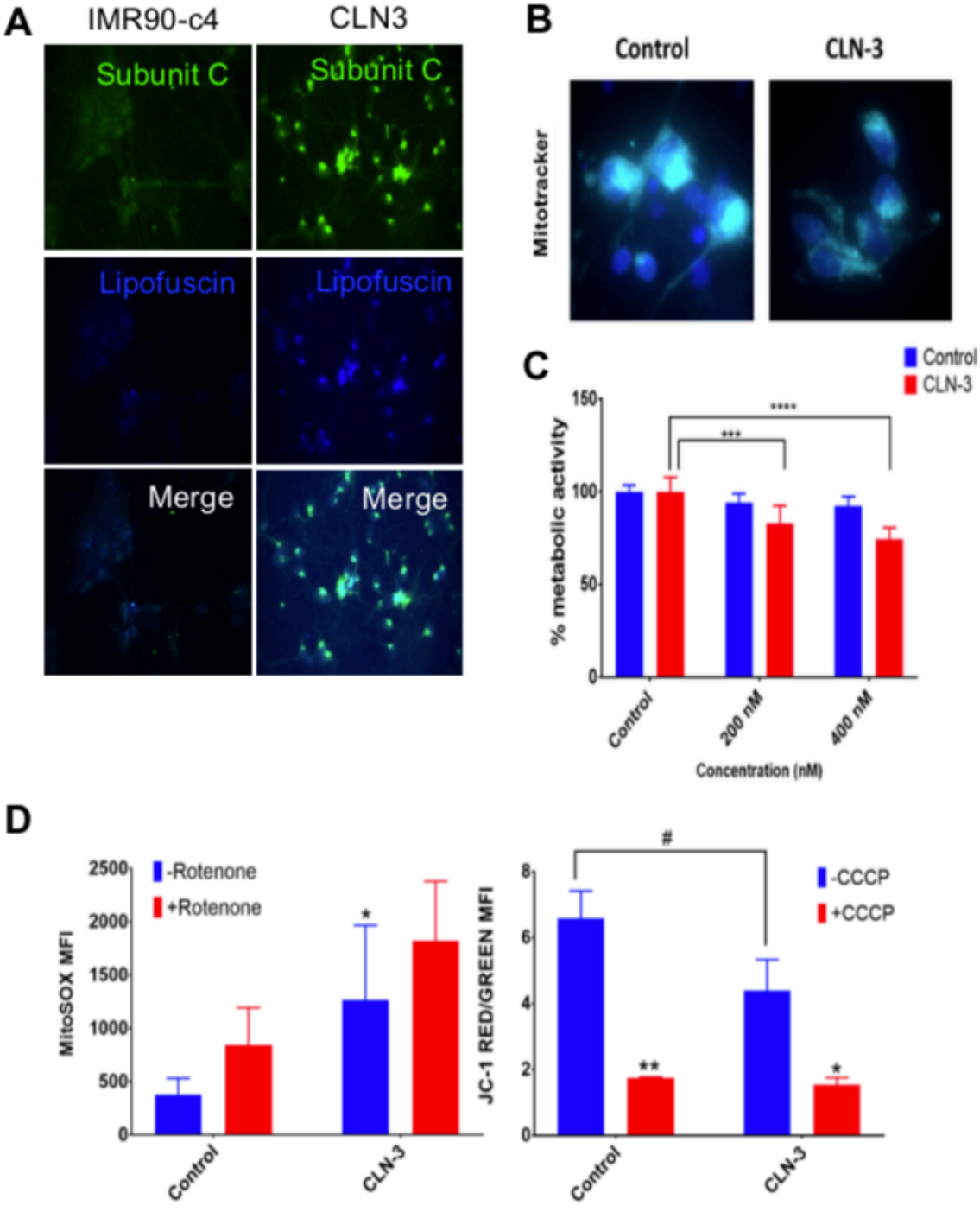
A
IMR90-c4
CLN3
Subunit C
Subunit C
Lipofuscin
Lipofuscin
Merge
Merge
B
Control
CLN-3
Mitotracker
C
Control
CLN-3
% metabolic activity
150
100
50
0
****
***
Control
200 nM
400 nM
Concentration (nM)
D
-Rotenone
+Rotenone
MitoSOX MFI
2500
2000
1500
1000
500
0
*
Control
CLN-3
#
-CCCP
+CCCP
JC-1 RED/GREEN MFI
8
6
4
2
0
**
*
Control
CLN-3

Figure 4: Phenotypical characteristic of iPSC-derived BMECs from the CLN3 line

(A) Simplified sketch representing the iPSC-derived BMECs differentiation protocol. (B) Representative micrograph pictures of iPSC-derived BMECs. Note the expression of vascular markers (PECAM-1, CDH5) in both iPSC lines, as well as the presence of BBB-specific markers (GLUT1, CLDN5 and OCLDN). (C) Expression profile of drug efflux transporters in both IMR90-c4-derived BMECs and CLN3-derived BMEC monolayers. DAPI staining is denoted in blue.


A
Undifferentiated iPSCs
Differentiating BMECs
Immature BMECs
Mature BMECs

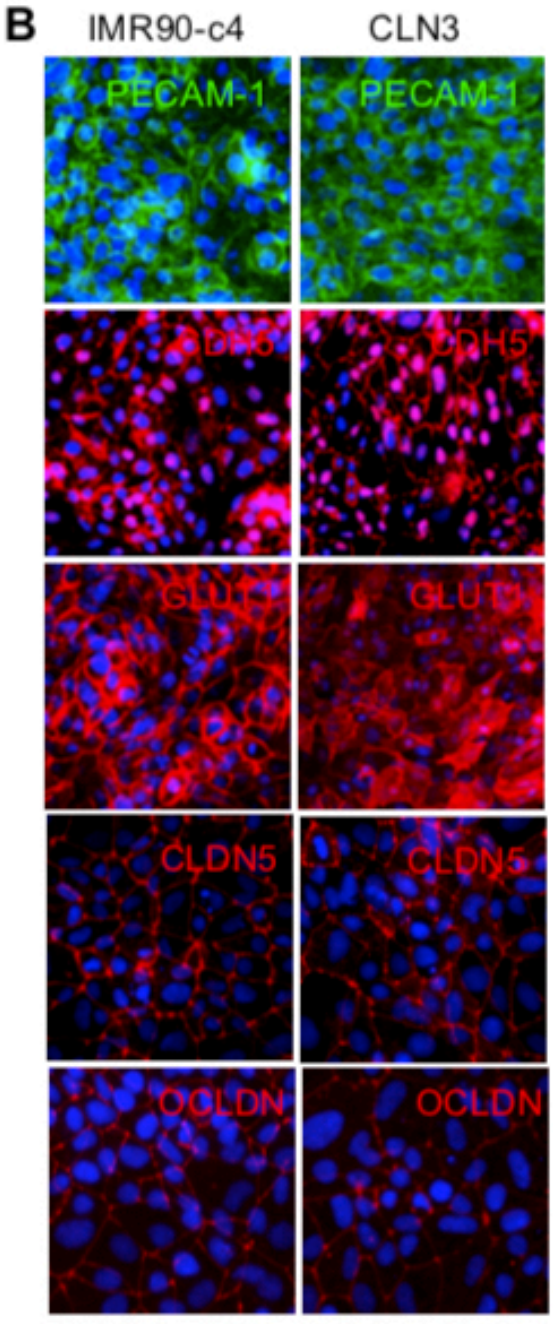
B
IMR90-c4
CLN3
PECAM-1
PECAM-1
CDH5
CDH5
GLUT1
GLUT1
CLDN5
CLDN5
OCLDN
OCLDN

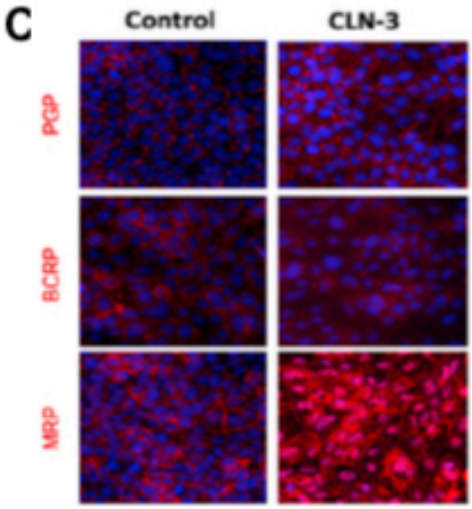
C
Control
CLN-3
PGP
BCRP
MRP

Figure 5: CLN3-derived BMECs display an impaired barrier phenotype.

(A&B) Measurement of transendothelial electrical resistance (TEER) and fluorescein permeability between IMR90-c4-derived BMECs (Control, blue bar) and CLN3-derived BMECs (red bar). (C) Additional maturation time (7 days UM combined with 6 days EC) in CLN3-derived BMECs failed to improve the barrier outcomes. (D) BMEC/neuron co-cultures impact the barrier outcome. (E) Protein expression profile of P-glycoprotein (P-gp), breast cancer resistance protein (BCRP) and multidrug resistance protein (MRP). (F) Drug efflux pump activity in iPSC-derived BMECs. (G) CLN3 mutation is associated with increased BSA and transferrin uptake between IMR90-c4-derived BMECs and CLN3-derived BMECs. (H) Temperature-dependent uptake of BSA and transferrin is more accentuated in CLN3-derived BMECs. (I) Immunoblot profile of clathrin and caveolin-1 (cav-1) expression in iPSC-derived BMECs. Band densities were normalized to actin. N=3/group, * denotes $P<0.05$, **$P<0.01$, ***$P<0.001$ and ****$P<0.0001$.

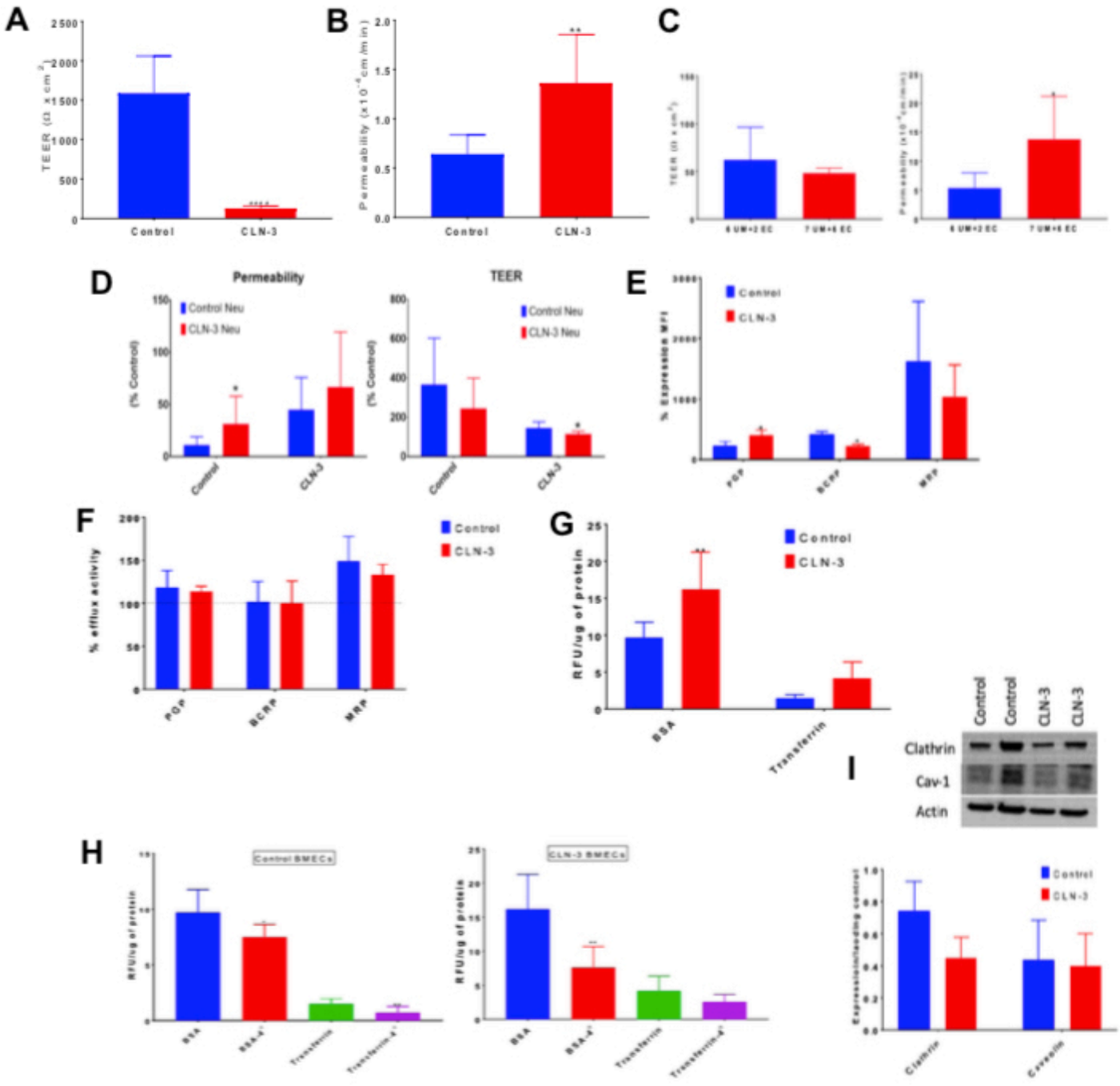
A
B
C
D
Permeability
TEER
Control Neu
CLN-3 Neu
E
Control
CLN-3
F
G
RFU/ug of protein
BSA
Transferrin
I
Control
Control
CLN-3
CLN-3
Clathrin
Cav-1
Actin
H
Control BMECs
CLN-3 BMECs

Figure 6: CLN3-derived BMECs show an abnormal angiogenic phenotype.

(A) Cell migration assay and (B) cell proliferation assay. Angiogenic assays were performed on iPSC-derived BMECs seeded on growth-factor reduced Matrigel® at a density of 10,000 cells/cm^2. Total tube length (C), number of nodes (D) and number of junctions (E) were quantified from images obtained (Supplementary Fig. 1A&B) at different time points. N=3/group, * denotes P<0.05, **P<0.01, ***P<0.001 and ****P<0.0001.

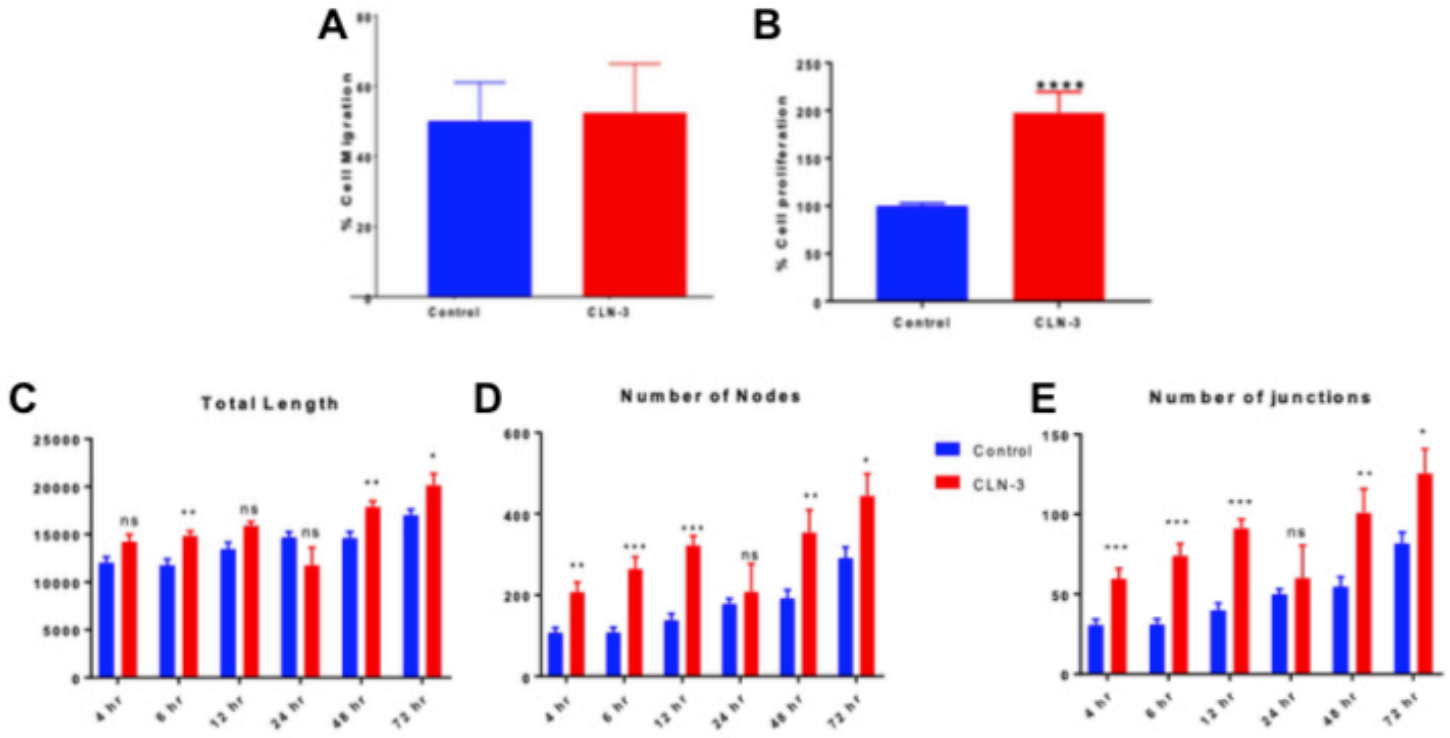
A
% Cell Migration
Control
CLN-3
B
% Cell proliferation
****
Control
CLN-3
C
Total Length
ns
**
ns
ns
**
*
4 hr
6 hr
12 hr
24 hr
48 hr
72 hr
D
Number of Nodes
**
***
***
ns
**
*
E
Number of junctions
Control
CLN-3
***
***
***
ns
**
*

Figure 7. Neuroprotective small molecules induce autophagy and Bcl-2 expression in CLN3-derived neurons.

A) Aromatic carbamates induce autophagy as measured by acridine orange stain. n = 3/cell line, expressed as mean ± SD. Rapa = rapamycin. One-way ANOVA; 95% Confidence Interval; *, $p<0.05$; ****, $p<0.0001$. B) Aromatic carbamates induce autophagy as measured by CytoID stain. n = 3/cell line, expressed as mean ± SD, *$p<0.05$, **$p<0.01$. C) Expression of autophagy related proteins by Western blot after treatment of CLN3-derived neurons with selected compounds (3 μM), rapamycin (Rapa, 0.5 μM) and rasagiline (Ras, 1 μM). Representative Western blot image. n = 2/cell line. Graphs represent quantification of Western blot data expressed as mean ± SD. D) Expression of subunit C of mitochondrial ATP synthase in untreated IMR90-c4-derived neurons (IMR90 Control), untreated CLN3-derived neurons (CLN3 Control), and CLN3-derived neurons treated with the indicated small molecules (3 μM) for 48 hours. Representative Western blot image. n = 2/cell line. Graph represents quantification of Western blot data expressed as mean ± SD. One-way ANOVA; 95% Confidence Interval; *, $p<0.05$.

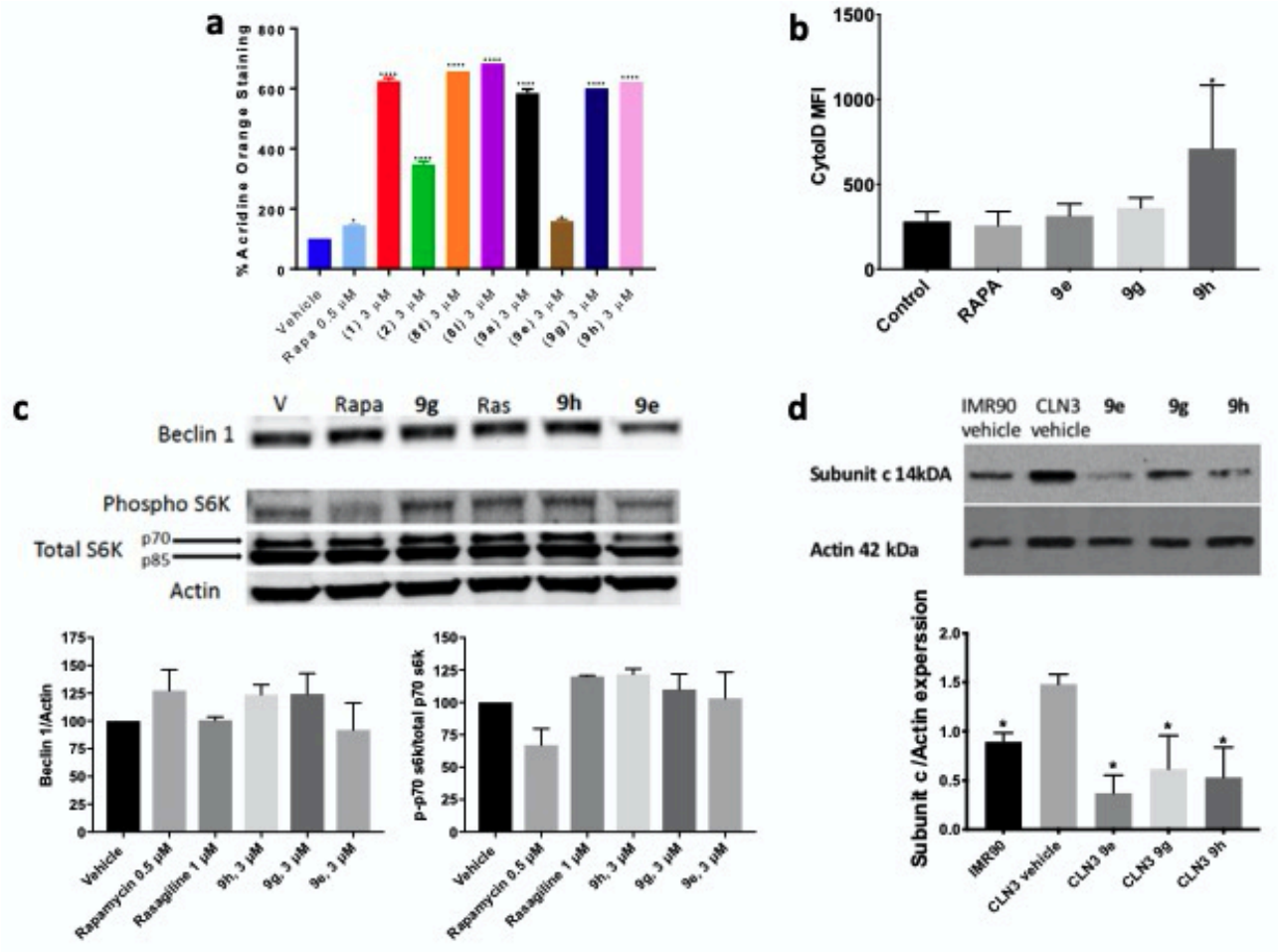
a
% Acridine Orange Staining
Vehicle
Rapa 0.5 μM
(1) 3 μM
(2) 3 μM
(6f) 3 μM
(6l) 3 μM
(9a) 3 μM
(9e) 3 μM
(9g) 3 μM
(9h) 3 μM
b
CytoID MFI
Control
RAPA
9e
9g
9h
c
V
Rapa
9g
Ras
9h
9e
Beclin 1
Phospho S6K
Total S6K
p70
p85
Actin
Beclin 1/Actin
Vehicle
Rapamycin 0.5 μM
Rasagiline 1 μM
9h, 3 μM
9g, 3 μM
9e, 3 μM
p-p70 s6k/total p70 s6k
d
IMR90 vehicle
CLN3 vehicle
9e
9g
9h
Subunit c 14kDA
Actin 42 kDa
Subunit c /Actin experssion
IMR90
CLN3 vehicle
CLN3 9e
CLN3 9g
CLN3 9h

Figure 8. Neuroprotective small molecules induce Bcl-2 expression in CLN3-derived neurons and rescue dysfunctional mitochondrial respiration in CLN3-derived NPCs.

A) Bcl-2 induction expressed as percentage of Bcl-2 change upon small molecule treatment of CLN3-derived neurons at 3 μM. n = 2, expressed as mean ± SD. One-way ANOVA; 95% Confidence Interval; *, p= <0.05; **, p= <0.01; ***, p= <0.001; ****, p= <0.0001. B) Mitochondrial Respiration of IMR90-c4-derived NPCs (blue bar), CLN3-derived NPCs (red bar), treated with rapamycin (0.5 μM) for 48 hrs (green bar) or **9e** (3 μM) for 48 hrs (purple bar) as determined by the mito stress test on a Seahorse extracellular flux analyzer. C) Quantification of Basal respiration, D) spare respiratory capacity and E) ATP production as determined by the mito stress test on a Seahorse extracellular flux analyzer. n = 3, expressed as mean ± SD. One-way ANOVA; 95% Confidence Interval; *, p= <0.05; ***, p= <0.001; ****, p= <0.0001.

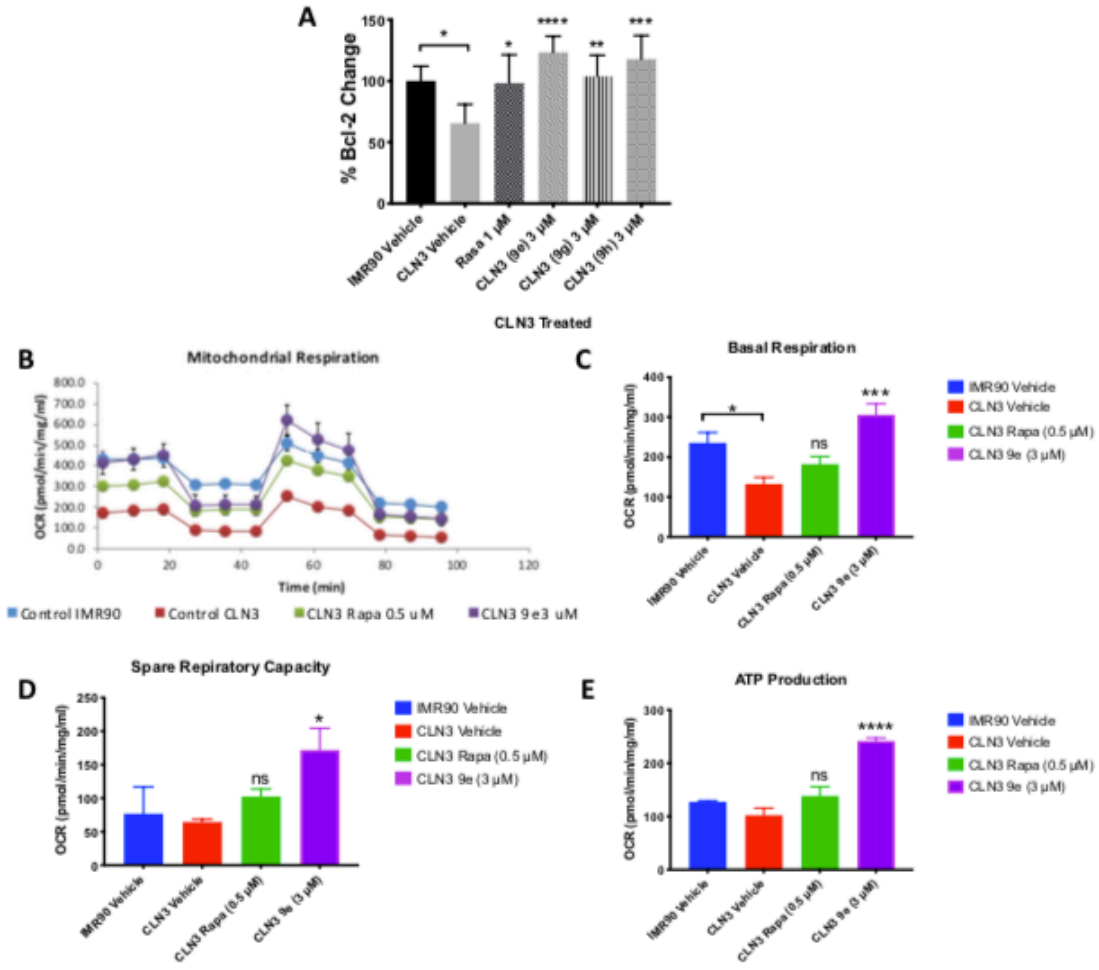
A
% Bcl-2 Change
IMR90 Vehicle
CLN3 Vehicle
Rasa 1 µM
CLN3 (9e) 3 µM
CLN3 (9g) 3 µM
CLN3 (9h) 3 µM
CLN3 Treated
B
Mitochondrial Respiration
OCR (pmol/min/mg/ml)
Time (min)
Control IMR90
Control CLN3
CLN3 Rapa 0.5 uM
CLN3 9e 3 uM
C
Basal Respiration
OCR (pmol/min/mg/ml)
IMR90 Vehicle
CLN3 Vehicle
CLN3 Rapa (0.5 µM)
CLN3 9e (3 µM)
ns
D
Spare Repiratory Capacity
OCR (pmol/min/mg/ml)
IMR90 Vehicle
CLN3 Vehicle
CLN3 Rapa (0.5 µM)
CLN3 9e (3 µM)
ns
E
ATP Production
OCR (pmol/min/mg/ml)
IMR90 Vehicle
CLN3 Vehicle
CLN3 Rapa (0.5 µM)
CLN3 9e (3 µM)
ns

SUPPLEMENTARY MATERIALS